Condensin loop extrusion properties, roadblocks, and role in homology search in *S. cerevisiae*

Author list

Vinciane Piveteau[1], Hossein Salari[1], Agnès Dumont[1], Jérôme Savocco[1], Chloé Dupont[1], Daniel Jost[1], Aurèle Piazza[1]

Affiliations

[1] Université de Lyon, ENS de Lyon, Université Claude Bernard, CNRS UMR5239, Laboratoire de Biologie et Modélisation de la Cellule, 46 Allée d'Italie, 69007 Lyon, France

Lead author: aurele.piazza@ens-lyon.fr

Abstract

The *in vivo* mechanism, regulations by *cis*-acting roadblocks, and biological functions of loop extrusion by eukaryotic SMC complexes are incompletely defined. Here, using Hi-C, we identified two condensin-dependent contact stripes at the Recombination Enhancer (*RE*) and the *rDNA* in *S. cerevisiae*. We show that oriented, unidirectional loop extrusion proceeds from these sites with an estimated processivity ~170 kb and a density ~0.04-0.18 that varies across the cell cycle. Centromeres and highly-transcribed RNA PolII-dependent genes are permeable condensin roadblocks. Other positionally labile elements such as replication forks and Smc5/6 complexes bound to substrates generated in the absence of Top2 also hinder loop extrusion by condensin. Cohesin is not an obstacle for condensin. Finally, a DNA double-strand break at *MAT* blocks condensin, which results in the rapid establishment of a long-range *RE-MAT* loop that juxtaposes the recombination machinery with its *HML*α donor target. Hence, all budding yeast SMCs are involved in recombinational DNA repair. We propose a revised model for donor selection during *MAT* switching that exploits specific properties of loop extrusion by condensin. It can serve as a paradigm for the establishment of other types of selective interactions along chromosomes.

Introduction

Most Structural Maintenance of Chromosome (SMC) family of ATPase complexes, including cohesin, condensin, and Smc5/6, share the ability to extrude DNA loops *in vitro* presumably via a conserved mechanism (Ganji *et al*, 2018; Davidson *et al*, 2019; Kim *et al*, 2019; Kong *et al*, 2020; Kim *et al*, 2020; Golfier *et al*, 2020; Pradhan *et al*, 2022; Shaltiel *et al*, 2022; Ryu *et al*, 2022; Pradhan *et al*, 2023; Janissen *et al*, 2024). Studying the function and activities of these complexes in cells has proven more challenging, as they generally do not have well-defined loading sites from which extrusion can be experimentally tracked. This is at the notable exception of the condensin-like bacterial SMC loading at *parS* sites (Gruber & Errington, 2009; Sullivan *et al*, 2009), and of a specialized condensin complex (condensin DC) loaded at *rex* sites on the X chromosome in XX hermaphrodites *C. elegans* animals (Morao *et al*, 2022), which enabled studying the loop extrusion activities of these SMCs and identify roadblocks *in vivo* with Hi-C (Morao *et al*, 2022; Brandão *et al*, 2021, 2019; Wang *et al*, 2017; Tran *et al*, 2017).

Condensin I and II are conserved SMC complexes specialized in chromosome assembly and segregation (Hirano, 2016). In *S. cerevisiae*, a single condensin complex individualizes mitotic chromosomes and promotes rDNA segregation at anaphase (Lazar Stefanita *et al*, 2017; Renshaw *et al*, 2010; Guérin *et al*, 2019; Freeman *et al*, 2000). It is also associated with chromatin at all cell cycle phases, suggesting roles outside of mitosis (Freeman *et al*, 2000; D'Ambrosio *et al*, 2008; Leonard *et al*, 2015). Recently, it has been involved in mating-type (*MAT*) switching (Li *et al*, 2019; Dinda *et al*, 2023), an event induced right prior or upon S-phase entry and that takes ~1 hour to complete (Nasmyth, 1983; Haber, 2012).

MAT switching is a specialized and highly efficient case of selection of specific chromosomal interactions in a competitive situation. As such, it represents a classic model for studying the mechanisms and regulations underlying the establishment of specific and exclusive interactions along chromosomes, such as between specific enhancers and promoters. It is a homologous recombination (HR)-dependent gene conversion event initiated by a site-specific DNA double-strand break (DSB) inflicted by the homothallic (HO) endonuclease at the transcribed *MAT* locus on chr. III (Haber, 2012). Gene conversion occurs using one of two silent donors carrying the opposite mating-type information: *HML*α and *HMR*a at the left and right extremity of chr. III, respectively. Of note, *MAT* is located ~95 kb away from *HMR*a on the same chromosome arm. Yet, *MAT*a cells efficiently use the more distant *HML*α donor present ~186 kb away across the centromere. Donor preference is regulated by a bipartite "recombination enhancer" (*RE*) element present ~14 kb away from *HML*α, only active in *MAT*a cells (Haber, 2012). The first part binds the Rad51-ssDNA filament in *trans* and promote homology search in its vicinity (Renkawitz *et al*, 2013; Dumont *et al*, 2024), and the second part is required for the horseshoe folding of chr. III, that brings the

left and right chromosomal arms in close proximity (Dekker *et al*, 2002; Belton *et al*, 2015; Li *et al*, 2019). This horseshoe folding depends on condensin, which is enriched at the *RE* in a Sir2-, Tof2-, Fob1-, cohibin-, and Mcm1-dependent manner only in *MAT*a cells, suggesting that it is loaded there (Li *et al*, 2019; Dinda *et al*, 2023). Accordingly, condensin and the proteins required for its enrichment at the *RE* promote usage of *HML*α upon DSB formation at *MAT*a (Li *et al*, 2019; Dinda *et al*, 2023). Such non-mitotic role of condensin has been ascribed to its chr. III folding activity.

A second condensin-enrichment site in the budding yeast genome, with largely overlapping requirements at the notable exception of the α2-repressible Mcm1 factor, is the replication fork barrier (RFB) within *rDNA* repeats (Johzuka & Horiuchi, 2009). These putative loading sites represent an opportunity to study the loop extrusion activity of condensin in eukaryotic cells and its function in establishing specific chromosomal interactions. Here, using Hi-C, we show the existence of a discrete condensin-dependent contact stripes emanating from the *RE* and the *rDNA* locus, and provide several lines of evidence that condensin unidirectionally extrudes chromatin loops from these sites with a defined orientation in cells. In conjunction with a simple, quantitative polymer model for loop extrusion, we exploit this system to determine the basic loop extrusion properties of condensin *in vivo* and delineate its regulation in *cis* by various types of roadblocks. Functionally, condensin loop extrusion properties are uniquely exploited in the donor selection process during *MAT* switching, upon conditional reconfiguration of chr. III structure.

Results

Two condensin-dependent contact stripes in the budding yeast genome

Chromatin immunoprecipitation (ChIP)-based assays revealed that the *RE* is the unique genomic region most enriched for condensin in *MAT*a cells (**Fig. 1A**) (Li *et al*, 2019; Costantino *et al*, 2020; Rossi *et al*, 2021). Such approaches cannot straightforwardly disambiguate loading and accumulation of long-range translocases such as SMCs, unlike Hi-C (Wang *et al*, 2017; Brandão *et al*, 2021; Wike *et al*, 2021; Guo *et al*, 2022; Morao *et al*, 2022; Kim *et al*, 2024). Previous Hi-C experiments failed to clearly established such contact signature at the *RE* (Belton *et al*, 2015; Li *et al*, 2019) while recent micro-C data indicated the presence of a contact stripe (Dinda *et al*, 2023). Our Hi-C protocol that yields contact maps at sub-kilobase resolution was applied on asynchronous population of haploid *MAT*a and *MAT*α cells. It confirmed the presence of a discrete contact stripe emanating from the *RE* and stretching across chr. III, which was specific to *MAT*a cells (**Fig. 1A**). It depended on the presence of the *RE*, as did the overall chr. III folding (**Fig. S1A**) (Belton *et al*, 2015). This stripe could be visualized as a 4C-like profile and compared to equivalent sites in the yeast genome (**Fig. S1B** and **Methods**), which revealed a specific enrichment of contacts from 40 kb to the end of chr. III (**Fig. 1B)**. These observations suggested that a heterogeneous population of loops link the *RE* and the rest of chr. III specifically in *MAT*a cells (Belton *et al*, 2015; Li *et al*, 2019; Dinda *et al*, 2023; Li *et al*, 2024). As for the *RE*, a contact stripe emanating from the left rDNA-flanking region and extending up to the centromere of chr. XII could be observed, exhibiting similar contact enrichment features independently of the mating type (**Fig. S1C**).

We addressed the dependency of these stripes on condensin by depleting its Smc2 subunit using the auxin-inducible degron (AID) system (Morawska & Ulrich, 2013) in an asynchronous culture of haploid *MAT*a cells (**Fig. 1C**). Condensin depletion did not affect the cell cycle distribution, the genome-wide probability of contact P_c as a function of genomic distance *s*, and only exhibited substantial changes in contacts on chr. III and XII (**Fig. S1D-F**) (Lazar□Stefanita *et al*, 2017; Costantino *et al*, 2020). The *RE*-borne stripe on chr. III was lost together with the *MAT*a-specific chr. III folding upon condensin depletion (**Fig. 1C-D**). The contact stripe emanating from the rDNA-flanking region and extending up to the centromere of chr. XII also depended on condensin independently of the mating type (**Fig. 1E** and **Fig. S1E-F**). No corresponding stripe was found on the telomere side of the rDNA (**Fig. S1F**), suggesting that loop formation by condensin is oriented. No other condensin-dependent stripe was observed genome-wide.

Finally, we addressed whether the *RE* was sufficient for forming a contact stripe outside of the context of chr. III by introducing it at an interstitial location on chr. IV (**Fig. 1F**). It resulted in the formation of a single stripe emanating from the *RE* insertion site and extending up to the right end of chr. IV specifically

in *MAT*a cells (**Fig. 1F-G**). This observation was corroborated upon introduction of the minimal right part of the *RE* that contains the condensin-enriched site but lacks the Fkh1-enriched domain (**Fig. S1G-H**) (Li *et al*, 2019; Haber, 2012). Hence, the *RE* is required and sufficient for forming a site-specific and directional contact stripe sensitive to the mating-type status.

These observations provide strong evidence that condensin extrude chromatin loops in *S. cerevisiae* cells. These loops have two well-defined anchors that correspond to highly enriched condensin binding sites: the *RE* and at the *rDNA*. They may be formed by two main scenario: an unidirectional loop extrusion process initiated at the site present at the base of the stripe; or from a site-specific block of loop extrusion events initiated at multiple dispersed sites (Fudenberg *et al*, 2016, 2017; Vian *et al*, 2018). In the following sections we assumed the first scenario to be correct. This assumption is supported by additional evidence presented below and summarized in the **Discussion**.

Density and processivity of loop extrusion by condensin inferred from biophysical modelling

We sought to infer properties of loop extrusion by condensin in cells by comparing experimental contact data with the output of a quantitative "scrunching" framework (**Fig. 1H**). It integrates the unidimensional stochastic motion of loop extruders along the chromosome into a simple polymer model to predict the impact of loop extrusion on contact frequencies, which can be compared to Hi-C contact data (Alipour & Marko, 2012; Sanborn *et al*, 2015; Fudenberg *et al*, 2016; Chan & Rubinstein, 2023). In this framework, condensin can bind and unbind to its loading site at rates k_b and k_u respectively. Upon binding, one leg of the condensin remains anchored at the binding site while the other translocates along the chromosome at a speed v_e. These parameters define two key observables: the processivity $p = v_e/k_u$, which describes the average loop size extruded by condensin in the absence of roadblock; and the density of loop extruders bound to DNA at any single time $d = k_b/(k_b + k_u)$. Pausing at site-specific roadblocks *i* can also be modeled. This allows to estimate the probability to observe an extruding loop between the condensin loading site and any other site along the chromosome and thus to predict their contact frequency. We first applied our framework to infer model parameters consistent with the uninterrupted stripe emanating from the *RE* inserted on chr. IV. This led to best-fitting parameters for condensin processivity in the ~150-210 kb range, with a density of condensin on chromatin d = 0.04 (**Fig. 1I** and **S1I**). Similarly, condensin-mediated loop extrusion proceeded with a processivity p = 120 kb and a density d = 0.11 from the *rDNA* and p = 150 kb and a density d = 0.06 from the *RE* in asynchronous cells. Consistently, the *SMC2-AID* control strain yielded similar p = 150-170 kb and d = 0.05-0.07, while Smc2 depletion caused a reduction of d = 0.02 at both sites without affecting p. These results indicate that

condensin is a chromatin loop extruder with processivity an order of magnitude greater than that of cohesin in *S. cerevisiae*.

The density of condensin-dependent loops is cell cycle-regulated

Although budding yeast condensin is detected on chromatin at all cell-cycle stages, its enrichment at specific genomic sites and its role in chromatin compaction and rDNA-*CEN12* tethering varies along the cell cycle (Lazar□Stefanita *et al*, 2017; Freeman *et al*, 2000; D'Ambrosio *et al*, 2008; Leonard *et al*, 2015; Bhalla *et al*, 2002). Consequently, we analyzed the loop extrusion by condensin on chr. III and XII in G1, S-phase, and in cells arrested in G2/M either artificially (*i.e.* repression of *CDC20* or addition of nocodazole) or upon activation of the DNA damage checkpoint (*i.e.* formation of an unrepairable site-specific DNA double strand break on chr. V), and determined best-fitting loop extrusion parameters for each condition (**Fig. 2** and **S2**). The contact stripes emanating from the *RE* on chr. III and the rDNA on chr. XII were detectable at all cell cycle stages, with phase-specific variations in intensity and pausing at centromeres (**Fig. 2** and **S2** and see below).

Cells arrested in G1 with alpha-factor exhibited a stripe signal similar to that of asynchronous cells on both chr. III and chr. XII (**Fig. 2A** and **S2B**). Consistently, best-fit parameters yielded p = 170 kb and d = 0.11 for the *rDNA* and p = 120 kb and d = 0.05 for the *RE*. Differently, the contact stripe on chr. III during S-phase failed to progress past ~120 kb (**Fig. 2B** and **S2C**), resulting in an altered chr. III conformation in which contacts between the left arm and the right arm distal to *MAT* strongly decreased (**Fig. S3A**). Likewise, the condensin extrusion span on chr. XII did not exceed ~80 kb. Simulations indicated a reduction of processivity (p = 80 kb and 30 kb at the *RE* and the *rDNA*, respectively) while loop density remained unchanged (d = 0.09-0.1). Hence, condensin translocation, but not loading, is inhibited during S-phase. Finally, the contact stripes were overall similar in G2/M and asynchronous cells on both chr. III and XII (**Fig. 2C-E** and **S2D-F**): the estimated processivity remained constant (p = 170 kb) while loop density d increased modestly at the *rDNA*, between 0.12 to 0.18 from 0.11 in G1. Hence, loop extrusion by condensin at these specific sites is active in mitosis prior to anaphase and presumably regulated at the loading stage, while its overall loop extrusion activity remains unaltered (Lazar□Stefanita *et al*, 2017; Guérin *et al*, 2019; Freeman *et al*, 2000; Leonard *et al*, 2015; Strunnikov *et al*, 1995).

Replication forks stall loop extrusion by condensin

The condensin loop extrusion span was stongly reduced on both chr. III and XII during S-phase (**Fig. 2B**). *RE*-bound loop extrusion initiates in an early-replicated region and progressed on chr. III up to the broad vicinity of *ARS310*, which corresponds to the first late replicating region encountered (**Fig. 3A**). Differently, the condensin loop extrusion initiates in an unreplicated region on chr. XII, and collapsed rapidly before encountering the first early-replicating *ARS1215* region. Since unreplicated DNA and pre-

replication complexes are not *per se* barriers to loop extrusion by condensin (*e.g.* G1-arrested cells **Fig. 2A**, **B**), we addressed whether replication forks are roadblocks for condensin by depleting the DNA replication initiation factor Cdc45 in G1-arrested cells and releasing them in S-phase (**Fig. 3B**). Preventing origins from firing restored condensin progression up to the end of chr. III and over ~ 200 kb on chr. XII (**Fig. 3B**), indicating that inactive replisome components on chromatin are not an obstacle to condensin. Differently, authorizing replication firing but immediately blocking replication forks progression at high hydroxyurea (HU) concentration further reduced the condensin loop extrusion span (**Fig. 3C** and **S3B-C**). The immediate blocking of replication forks upon HU treatment further allowed visualizing discrete loop extrusion pausing at the level of replication origins (**Fig. 3D**). Hence, replication forks are condensin translocation roadblocks, independently of replisome progression.

Smc5/6 inhibits condensin-mediated loop extrusion in the absence of Top2

Top2 promotes loop extrusion by Condensin DC in *C. elegans* (Morao *et al*, 2022) and condensin function in chromosome compaction is tightly coupled to Top2 activity in bacteria and eukaryotes (Hirano, 2016). We thus addressed whether condensin translocation requires Top2 activity by re-analyzing published Hi-C datasets of cells arrested in mitosis upon treatment with benomyl in which Top2 was either conditionally inactivated at restrictive temperature (*top2-4* (Holm *et al*, 1985)) or depleted (Top2-AID) upon auxin addition prior to S-phase entry and up to mitotic arrest (Jeppsson *et al*, 2024) (**Fig. 4A** and **S4A**). The span of loop extrusion by condensin was reduced on both chr. III and chr. XII in the absence of Top2 activity, with a slightly more penetrant phenotype upon Top2 heat inactivation than Top2 depletion (**Fig. 4A** and **S4A**). These results show that Top2 promotes loop extrusion by condensin.

The loop extruding Smc5/6 complex (Pradhan *et al*, 2023) mainly associates with chromatin following S-phase (Jeppsson *et al*, 2014). Condensin association with chromatin is increased upon Top2 inhibition, and has recently been shown to be targeted at positively supercoiled chromatin regions (Jeppsson *et al*, 2024). Consequently, we investigated the contribution of Smc5/6 to condensin-mediated loop extrusion and pausing by re-analyzing Hi-C datasets in which members of the Smc5/6 complex (Smc5, Smc6, Nse4 and/or Nse5) were depleted in otherwise WT or Top2-deficient conditions (Jeppsson *et al*, 2024). Depletion of Smc5/6 alone did not affect loop extrusion by condensin (**Fig. 4B** and **S4B-C**). However, Smc5/6 depletion partly relieved the barrier for loop extrusion observed in the absence of Top2 (**Fig. 4C** and **S4D**). This restoration of extrusion occurred over ~200 kb on chr. XII and, to a lesser extent, over the whole chr. III (**Fig. 4C** and **S4D**). Since Smc5/6 loads at, and remains associated with positive supercoils (Jeppsson *et al*, 2024), these results suggest that topological structures bound by Smc5/6 are roadblocks for condensin translocation along chromosome arms.

Determinants of the condensin roadblock at centromeres

To gain insights into the nature and determinants of the condensin loop extrusion pausing at centromeres (**Fig. 1**), we related the roadblock at *CEN3* to the folding of the peri-centromeric regions across the cell cycle (**Fig. 5A**). No clear roadblock was detected in G1, consistent with the lack of condensin at peri-centromeres (Leonard *et al*, 2015). A narrow roadblock appeared in S-phase, and became highly prominent in metaphase-arrested cells. This roadblock at the centromere was still observed upon treatment of cells with the microtubule-depolymerizing drug nocodazole, indicating it is independent of the mitotic spindle and of centromere clustering (**Fig. 5B**). Furthermore, Cdc45-depleted cells that reach metaphase in the absence of replication, and thus lack the sister chromatid required for the spindle to exert tension, also retained a localized roadblock (**Fig. 5C**). Roadblock appearance coincided with S-phase, when loop extruding cohesins starts to be loaded (Costantino *et al*, 2020; Dauban *et al*, 2020) and structure the peri-centromere (Yeh *et al*, 2008; Paldi *et al*, 2020). The role of cohesin in blocking condensin was addressed upon Scc1 depletion in G1-arrested cells and its effect determined in the following S-phase and metaphase. The condensin roadblock persisted at the centromere (**Fig. 5D**) and condensin-dependent stripes along chromosome arms remained unaffected upon Scc1 depletion (**Fig. S5A-D**). Consequently, the centromeric roadblock for condensin is independent of spindle tension, centromere clustering, cohesin and centromere replication. More broadly, condensin is oblivious to the presence of cohesin on chromatin.

We then addressed whether the centromeric function was required to block condensin in *cis*. To this end, we specifically inactivated the centromere of chr. III upon inducible transcription across *CEN3* using the *pGAL-CEN* system (**Fig. 5E**) (Hill & Bloom, 1987). Such system causes the loss of the centromere-specific Cse4-containing nucleosome, and thus of the kinetochore, from *CEN3* (Nakabayashi & Seki, 2022). *CEN2* inactivation was used as a control (**Fig. S5E-G**). Strong transcriptional activation for 2 hours upon galactose addition caused a specific loss of contacts between the transcribed centromere and the 15 other centromeres, which was not restored after a 10 minutes transcriptional shutoff with glucose (**Fig. S5E**). The appearance and disappearance of the border pattern typical of highly-transcribed genes (Banigan *et al*, 2023; Chapard *et al*, 2023; Salari *et al*, 2024) confirmed the efficient transcriptional activation and shutoff (**Fig. S5F**). The centromeric roadblock was abolished upon *CEN3* transcription and rapidly recovered following transcriptional shutoff (**Fig. 5E**). Transcription across *CEN2* did not affect the roadblock at *CEN3* (**Fig. S5G**), indicating that the effect observed upon *CEN3* inactivation occurs in *cis*. Furthermore, the roadblock was lost in a strain defective for the dispensable outer kinetochore component Chl4, both in the presence and absence of spindle tension (**Fig. 5F**). These results indicate that the condensin roadblock at the centromere depends on the presence of the kinetochore in *cis*, irrespective of its role in mediating spindle tension and centromere clustering.

Highly transcribed RNA PolII genes transiently stall condensin translocation

Besides centromeres, the contact stripes on chr. III and XII exhibited local contact variations suggestive of the presence of additional roadblocks along chromosome arms, which could be highlighted upon contacts detrending (**Fig. S6A**). These positions were compared to various genomic and chromatin features detected by ChIP-Exo (Rossi *et al*, 2021) (**Fig. 6A**). Clearly, loop extrusion paused immediately ahead of sites enriched for RNA PolII, which exhibit the conserved "boundary" Hi-C pattern typical of highly-transcribed genes (**Fig. 6A**) (Banigan *et al*, 2023; Chapard *et al*, 2023; Salari *et al*, 2024). These profiles were also observed in G1- and metaphase-arrested cells (**Fig. S6B**). The pause site ~160 kb away from the rDNA and not associated with a RNA PolII-enriched site (**Fig. 6A**) corresponded to the region immediately upstream of the *GAL2* gene, specifically activated in our galactose-containing culture conditions (**Fig. 6A-B**; galactose did not change the expression of the other genes in the *CEN12-rDNA* interval, see (Pelechano *et al*, 2013) and **Fig. S6D** below). Accordingly, the boundary Hi-C pattern is readily detected at *GAL2* and other *GAL* genes (**Fig. 6A-B** and **S6B**). Cells grown in the presence of glucose did not exhibit the boundary nor the increased *rDNA-GAL2* looping (**Fig. 6B-C** and **S7**C). Transcriptional induction by addition of galactose for only 10 minutes was sufficient to induce transcription of the *GAL* genes and enrich for the *rDNA-GAL2* loop (**Fig. 6C** and **S6D-E**). Conversely, repression of *GAL* genes upon glucose addition to galactose-containing media for 10 minutes caused a partial loss of the *rDNA-GAL2* loop. Hence, condensin pausing ahead of a highly-transcribed PolII gene can be rapidly established and reversed, suggesting it is a primary consequence of its transcriptional activity. Pausing occurrs irrespectively of the gene orientation relative to the directionality of loop extrusion (*e.g. PDC1* and *PGK1* vs. *AHP1* and *GAL2* in **Fig. 6A**).

Inactivation of RNA PolII, either upon heat-inactivation of its Rpb1 subunit or upon thiolutin treatment, exerted profound effects on chromosome organization (Jeppsson *et al*, 2022), which prevented us from determining the compounded role in regulating the processivity of loop extrusion by condensin over large chromosomal segments.

DSB-dependent reconfiguration of chr. III structure promotes interaction between *MAT* and the *RE*

What is the functional significance of the condensin-mediated loop extrusion spanning across chr. III? Previous report revealed that condensin promoted usage of the *RE*-proximal *HML*α donor during *MAT* switching in *MAT*a cells, which was presumed to originate from its role in chr. III folding (Li *et al*, 2019; Dinda *et al*, 2023). Differently, we sought to address whether a DSB induced at *MAT* may act as a condensin roadblock, with the resulting *RE-MAT* loop directly juxtaposing the DSB to the *HML*α donor. To this end, we induced HO expression from a galactose-inducible promoter in asynchronous *MAT*a and

*MAT*α cells. Repair-deficient *rad51Δ* mutants were used to (i) ensure isolation of an homogeneous population bearing a DSB in a *MAT*a context (*i.e.* no switching to α), and (ii) prevent the Rad51-dependent preferential recruitment of the DSB to the *RE* in *trans* (Renkawitz *et al*, 2013; Dumont *et al*, 2024). Clearly, condensin translocation was blocked ahead of the DSB (**Fig. 7A-D**). Contacts passed the DSB region were not different from control sites, indicating that condensin cannot bypass the DSB (**Fig. 7B**). This *RE*-DSB loop organization leaving out the right chromosomal fragment has two consequences: it both promoted interaction between the DSB region and *HML*α, and reduced its interaction with *HMR*a (**Fig. 7D, E**). Hence, formation of a DSB at *MAT* leads to a condensin-dependent spatial reorganization of chr. III that poises the HR machinery to repair using the *HML*α donor (**Fig. 7H**).

Notably, no stripe anchored at the DSB nor a *CEN3*-DSB loop were observed 2 hours post-DSB induction (**Fig. 7A**, **D-E**). Hence, the loop extrusion reaction that connects the *RE* and the DSB does not detectably occurs in the reverse orientation (*i.e.* initiated at the DSB and moving towards the *RE*).

Finally, a stripe emanating from the *RE* and stretching up to the DSB site appeared 4 hours post-DSB induction in *MAT*α cells, bringing the DSB in close proximity to *HML*α (**Fig. 7A, F, G** and **S7C**). This re-establishment occurred after the elimination of the *MAT*α genes by resection (**Fig. 7A**), whose α2 gene product represses condensin loading at the *RE* (Li *et al*, 2019; Dinda *et al*, 2023). Hence, the active repression of condensin loading at the *RE* in *MAT*α cells provides a back-up redirection of homology search towards *HML*α in case of a failure to repair using the primary *HMR*a donor.

Discussion

Here, we provided evidence that condensin can be loaded at two specific sites in the budding yeast genome, from which it extruded chromatin loops. These unique loading sites enabled us to straightforwardly infer condensin loop extrusion properties and identify several roadblocks in cells. We propose a revised model of donor selection during *MAT* switching that exploits the specificities of loop extrusion by condensin.

Loop extrusion by condensin in *S. cerevisiae*

Contact stripes detected by Hi-C correspond to a heterogeneous population of loops sharing a discrete anchor. Such loop may be formed by a unidirectional extrusion process initiated at the loading site present at the base of the stripe, or by a site-specific block for extrusion processes randomly initiated at dispersed sites (Fudenberg *et al*, 2016, 2017; Vian *et al*, 2018). We present here arguments in favor of the first "loading" scenario. Indeed, in the "blocking" scenario, the numerous putative on-going loop extrusion events that have not yet reached the blocking site are expected to nonetheless link distant sites along the main Hi-C diagonal. Condensin removal should thus affect the probability of contact P_c as a function of genomic distance *s*, which was not observed (**Fig. S1E**). This absence of an effect on the genome-wide $P_c(s)$ could not be explained by distributed loading events only on chr. III and in the *CEN12-rDNA* intervals either, as a stripe could be observed by introducing the *RE* on chr. IV (**Fig. 1F-G)**. Finally, the *RE-MAT* loop specifically established upon DSB formation is only associated with a single stripe emanating from the *RE* (**Fig. 7E**). A single stripe is specifically predicted by the "loading" model while the "blocking" model predicted the appearance of a second stripe anchored at *MAT*. These multiple lines of evidence demonstrate that condensin is loaded at the RE, from which it unidirectionally extrudes loops, consistent with its activity *in vitro* on naked DNA (Ganji *et al*, 2018; Kim *et al*, 2020; Shaltiel *et al*, 2022).

Condensin extrudes loops with a broadly defined processivity of ~150-200 kb, which does not substantially vary between the G1 and G2/M phases. Condensin loading is modestly decreased in G1, consistent with its overall reduced presence on chromatin and the reduced amount of its limiting Ycg1 component at that cell cycle phase (D'Ambrosio *et al*, 2008; Leonard *et al*, 2015; Doughty *et al*, 2016). Importantly, loop extrusion by condensin from its loading sites has a defined orientation, leading to a single stripe, as observed at the *rDNA* or upon introduction of the *RE* on chr. IV (**Fig. 1F**). The mechanism ensuring this orientation remains to be determined: it may be directly imposed at the loading step, or result from a specific repression in *cis* of loop extrusion proceeding in the "wrong" orientation.

Roadblocks for loop extrusion by condensin

Various high-affinity DNA-bound elements such as dCas9, nucleosomes, dense arrays of the telomere-binding protein Rap1 or large nanoparticles transiently stall or block DNA loop extrusion by budding yeast condensin *in vitro* (Pradhan *et al*, 2022; Analikwu *et al*, 2023). Accordingly, telomeric arrays were implicated in blocking condensin translocation in *S. cerevisiae* (Guérin *et al*, 2019; Analikwu *et al*, 2023). Here we identify several additional discrete and dispersed condensin roadblocks of varying intensity: centromeres, highly-transcribed PolII genes, replication forks, Smc5/6 specifically in the absence of Top2, and DNA double-strand breaks (**Fig. 7I**). Centromeres and genes highly transcribed by RNA PolII can be bypassed with variable rates. Since RNA PolII stalls fission yeast condensin (Lebreton *et al*, 2024) that highly transcribed operons stall the condensin-like SMC in *B. subtilis* (Gruber & Errington, 2009; Brandão *et al*, 2019), and that the effect of transcription can be induced and reversed in less than 10 minutes (**Fig. 6C-D**) we suspect that basic aspects of transcription (or of its direct consequences on chromatin topology) hinder condensin translocation. Cohesin, which is also impeded and/or dynamically localized by RNA PolII in distantly-related eukaryotes (Lengronne *et al*, 2004; Busslinger *et al*, 2017; Valton *et al*, 2022; Banigan *et al*, 2023), does not detectably stall condensin.

Condensin and topoisomerase II collaborate for chromatid condensation and decatenation for their segregation at mitosis (Wood & Earnshaw, 1990; Hirano, 2016; Goloborodko *et al*, 2016; Racko *et al*, 2018; Orlandini *et al*, 2019; Dyson *et al*, 2021). We found that Top2 activity is required for condensin-mediated loop extrusion (**Fig. 4**). It parallels recent observations for the X-specific condensin DC in *C. elegans* (Morao *et al*, 2022), suggesting a broad conservation of a requirement for topological simplification for condensin function. This impairment, however, is not a direct consequence of topological alterations formed in the absence of Top2, but instead depends on the conserved Smc5/6 complex. Smc5/6 has recently been shown to load onto, and accumulate at the base of positive supercoils (Jeppsson *et al*, 2024). The physiological relevance and precise mechanism of this unsuspected regulation of condensin by Smc5/6 remains to be determined.

Finally, contexts in which the linearity of the dsDNA substrate is compromised are obstacles for condensin, such as a DSB or replication forks, as observed for cohesin (Piazza *et al*, 2021; Arnould *et al*, 2021; Jeppsson *et al*, 2022; Arnould *et al*, 2023). The loss of the origin-firing factor Cdc45 relieved the S-phase-specific blocking of condensin-mediated extrusion while forks stalling in the presence of HU prevented condensin motion (**Fig. 3**). Since MCM complexes are associated with pre-replication complexes independently of Cdc45 (Costa & Diffley, 2022), they are unlikely to be direct condensin roadblocks. This is in contrast to the inhibition they pose for cohesin translocation in mammalian cells (Dequeker *et al*, 2022). Further studies will be required to address the role in condensin translocation inhibition by putative replisome components and DSB-associated proteins. Alternatively, the inability of condensin to bypass a replication fork or a DSB may originate from a basic requirement for a single,

continuous substrate during the condensin translocation cycle (Shaltiel *et al*, 2022). To the best of our knowledge, this possibility has not yet been addressed with purified SMC complexes *in vitro*.

The relevant role of condensin in *MAT* switching is to form a *RE*-DSB loop

Homology search has primarily been understood as a 3D diffusive process (Bell & Kowalczykowski, 2016; Renkawitz *et al*, 2013; Wiktor *et al*, 2021; Liu *et al*, 2023; Dumont *et al*, 2024). In this framework, the *MAT*a-specific and RE-dependent conformation of chr. III has been presumed to facilitate search and bias donor usage by reducing the average distance between the DSB and its target *HML*α donor (Coïc *et al*, 2006; Belton *et al*, 2015; Lassadi *et al*, 2015; Li *et al*, 2019; Dinda *et al*, 2023). Here, we show that upon DSB formation condensin promiscuously and specifically associates *MAT*a and the *RE*, located ~170 kb away. Accordingly, increased proximity between *MAT* and the *RE* has been previously observed cytologically within 1 hour of DSB induction, but whether it resulted from the recombination process itself, or whether it preceded it, was not established (Simon *et al*, 2002; Avşaroğlu *et al*, 2016; Houston & Broach, 2006). Here we show that this association takes place in the absence of Rad51, indicating that it is not a consequence of homology search or of the Rad51-dependent recruitment of the DSB at the *RE* (Renkawitz *et al*, 2013; Dumont *et al*, 2024). The condensin-mediated clamping of the DSB and the *RE* is expected to limit their diffusion. Consistently, the diffusion coefficient of the chromatin flanking the *MAT* locus rapidly decreases following DSB induction (Saad *et al*, 2014), unlike DSBs formed on other chromosomes (Dion *et al*, 2012; Miné-Hattab & Rothstein, 2012). Functionally, such clamping should promote the over-sampling of the *RE*-surrounding region and considerably accelerate *HML*α identification (**Fig. 7J**). Accordingly, artificial tethering between *HML*α- and *MAT*α-adjacent sites could partially outcompete usage of *HMR*a (Simon *et al*, 2002; Kostriken & Wedeen, 2001), with a magnitude similar to that contributed by condensin in *HML*α usage in *MAT*a cells (Li *et al*, 2019; Dinda *et al*, 2023).

In this clamping model, the horseshoe folding of chr. III is an epiphenomenon resulting from futile cycles of loop extrusion by condensin, whose relevant role is to poise *MAT*a for rapid loop establishment with the *RE* upon DSB formation (**Fig. 7H**). Such conditional *RE*-DSB clamping is made uniquely possible by the properties of loop extrusion by condensin we defined here: its site-specific loading at the *RE*, its unidirectionality, its processivity (~170 kb), and its inability to bypass a DSB. Finally, the dependence of condensin loading at the *RE* on the α2-repressible Mcm1 protein (Dinda *et al*, 2023) provides a back-up homology search redirection system in *MAT*α cells in case of a prolonged failure to repair using the preferred *HMR*a donor. *MAT* switching thus provides a model to study the mechanism and regulations of the establishment of selective interactions between chromosomal segments.

All budding yeast SMCs are involved in recombinational DNA repair

Budding yeast encodes four structurally related SMC complexes: cohesin, condensin, Smc5/6, and Mre11-Rad50-Xrs2 (MRX). MRX is involved in DSB sensing and end-tethering, DNA damage checkpoint activation, and the initial resection event directing the repair towards HR (reviewed in (Cejka & Symington, 2021)). Cohesin is loaded and accumulates in a broad region surrounding the DSB following resection initiation in both *S. cerevisiae* and human cells (Kim *et al*, 2002; Ström *et al*, 2004; Ünal *et al*, 2007; Heidinger-Pauli *et al*, 2008; Bauerschmidt *et al*, 2010; Caron *et al*, 2012; Kong *et al*, 2014; Piazza *et al*, 2021; Scherzer *et al*, 2022). It also folds chromatin into loops genome-wide as cells arrest at metaphase in response to the activation of the DNA damage checkpoint in *S. cerevisiae* (Piazza *et al*, 2021). Functionally, cohesin regulates the homology search step of HR by promoting engagement of chromatin in *cis* and inhibits it in *trans* (Covo *et al*, 2010; Piazza *et al*, 2021; Dumont *et al*, 2024). Finally, Smc5/6 has been implicated in the repair of stalled or collapsed replication forks by HR (Peng & Zhao, 2023), as well as in DSB end-tethering (Phipps *et al*, 2023). Here, we revealed a direct role for condensin in promoting homology encounter specifically with one of two competing donors during HR in the specialized context of *MAT* switching. Accordingly, deficiency of condensin or of its loading at the *RE* causes a partial defect in *MAT* switching (Li *et al*, 2019; Dinda *et al*, 2023). Hence, all SMCs are involved in specific or general aspects of recombinational DNA repair in mitotically-dividing *S. cerevisiae* cells. It suggests a primordial role for SMCs in facilitating the uniquely challenging search between two unique and sub-diffusive chromatin segments.

Mechanistically, cohesin in *S. cerevisiae* and RecN in *C. crescentus* (Piazza *et al*, 2021; Chimthanawala *et al*, 2022; Dumont *et al*, 2024) were proposed to endow the RecA/Rad51-ssDNA filament with the ability to undergo long-range and directional 1D sliding on chromatin in *cis* from the break site (**Fig. 7J**). To achieve such scanning, SMCs must anchor at or near the RecA/Rad51-ssDNA filament and pump chromatin unidirectionally from that anchor. In this framework, SMC's processivity determines the range of preferential scanning while SMC's density determines the frequency of passage of the filament over that region. Such strategy may not be limited to SMCs, as a similar role in promoting 1D scanning on naked dsDNA *in vitro* has been reported for Rad54, a Rad51-associated Swi2/Snf2 translocase (Crickard *et al*, 2020; Hu & Crickard, 2024). Differently, condensin does not initially anchors at the break site, and thus does not promote scanning of chromatin in *cis*. Instead, it promotes a specific interaction between the region surrounding its loading site (*i.e.* the *RE*) and the break site located in its processivity range (**Fig. 7J**). Hence, distinct SMC loop extrusion properties are exploited to promote different search strategies: long-range scanning for cohesin and focal search for condensin.

Acknowledgements

We thank members of the Piazza, Bernard and Jost laboratories, as well as Armelle Lengronne, Frédéric Beckouët, and Romain Koszul for helpful discussions. We are grateful to Pascal Bernard, Armelle Lengronne, and Stéphane Marcand for their critical reading of the manuscript, and Rodney Rothstein, Thomas Guérin and Stéphane Marcand for sharing yeast strains.

This research was supported by the European Research Council (ERC) under the European Union's Horizon 2020 to A.P. (ERC grant agreement 851006) and the Agence Nationale de la Recherche to AP and DJ (ANR-23-CE12-0014-02).

Author contributions

Conceptualization: AP; Experiments: VP, JS, AD, CD, AP; Data analysis: AP; Modeling: HS, DJ; Data interpretation: HS, DJ, AP; Supervision: DJ, AP; Funding Acquisition: DJ, AP; Manuscript - Writing: AP; Manuscript – Editing: HS, DJ.

Declaration of interest

The authors declare no conflict of interest.

Figure legends

Figure 1: Condensin- and *RE*-dependent contact stripes in *MAT*a cells.

(A) Hi-C contact maps (left) and ratio map (right) of chr. III in exponential cultures of *MAT*a (APY142; merge of 5 biological replicates) and *MAT*α (APY295; merge of 2 biological replicates) cells. Calibrated ChIP-Exo profiles are from ref. (Rossi *et al*, 2021). Bin = 1 kb.

(B) Top: 4C-like contact profile of the *RE* (orange) and of the average of 6 control sites (black, see **Methods** and **Fig. S1B**) in *MAT*a and *MAT*α cells, from Hi-C data in (A). Data are smoothed over a 10 kb sliding window. Bottom: Ratio of *MAT*a and *MAT*α profiles.

(C) Top: Smc2 depletion scheme from an exponential culture of *MAT*a cells (YTG155), and validation of the Smc2-9Myc-AID depletion by western blot. Bottom: Hi-C contact maps and ratio maps of mock-treated and Smc2-depleted cells.

(D) Same as in (B) for data in (C).

(E) Same as in (D), but with the left rDNA-flanking region as a viewpoint, and the average of 6 control sites.

(F) Hi-C contact maps (left) and ratio map (right) of chr. IV containing an insertion of the *RE* at position 680 kb in *MAT*a and *MAT*α cells (APY1846 and APY1848, respectively).

(G) Top: 4C-like contact profiles of data in (F) and in a *MAT*a strain lacking the insertion of the *RE* on chr. IV (from data in (A)). Bottom: ratio of contacts in *MAT*a over *MAT*α cells in strains with and without insertion of the *RE* on chr. IV.

(H) Rationale of the unidirectional loop extrusion crunching model, parameters, and output.

(I) Contact frequencies obtained with the loop extrusion crunching model with varying processivity. Density was set to 0.04.

Figure 2: Regulation of loop extrusion by condensin across the cell cycle.

RE and rDNA-flanking 4C contact stripes (A) upon G1-arrest (APY266), (B) during S-phase (APY539 and APY607, merged), (C) upon metaphase-arrest due to *CDC20* repression (APY537), (D) upon DDC-induced metaphase-arrest due to formation of a single unrepairable HO-induced DSB at *ura3* (APY266), and (E) upon mitotic-arrest in the presence of nocodazole (APY266). All cells are *MAT*a. The number of biological replicates n is indicated. The loop extrusion span is schematized by a line. Best-fitting simulation processivity (p) and density (d) values are indicated. Other legends as in **Fig. 1B**.

Figure 3: Replication forks block loop extrusion by condensin.

(A) Top: Hi-C coverage in S-phase. Bottom: *RE* and rDNA-flanking contact stripes in S-phase over that of asynchronous cultures (n=5 from **Fig. 1A**). Data smoothed over 10 kb.

(B) Entry in S-phase in the absence of replication origin firing partially restores loop extrusion by condensin on chr. III and XII (APY607). n = 1 biological replicate. Data smoothed over 10 kb.

(C) Stopping replisome progression immediately after S-phase entry prevents loop extrusion by condensin. n = 3 biological replicates. Data are from ref. (Jeppsson *et al*, 2022). Contact frequencies smoothed over 10 kb. Coverage smoothed over 4 kb.

(D) Zoom on data in (C). Data smoothed over 4 kb overlaid onto mean ± SEM.

Figure 4: Smc5/6 blocks condensin translocation in Top2-deficient cells.

(A) Top2 deficiency inhibits loop extrusion by condensin. Top: experimental schemes. Middle and bottom: Condensin-dependent *RE* and rDNA-flanking contact stripes in Top2-deficient and WT cells and their ratio.

(B) Smc5/6 depletion does not affect loop extrusion by condensin. Legend as in (A)

(C) Depletion of Smc5/6 partially suppresses the inhibition of condensin-mediated loop extrusion in the absence of Top2. Legend as in (A).

(A-C) Data from ref. (Jeppsson *et al*, 2024), smoothed over 10 kb. n: number of biological replicates.

Figure 5: The centromere stalls condensin translocation in a kinetochore-dependent manner.

(A) Condensin roadblock at *CEN3* across the cell cycle. Top: Hi-C maps of the *CEN3*-surrounding region. Middle: Aggregated contact maps of all centromeres. Bottom: *RE*-contact stripes. Window size is ±40 kb. Data smoothed over 4 kb overlaid onto mean ± SEM. Data are from **Fig. 2A-E**.

(B) Legends as in (A). n = 2 biological replicates for DSB 4h + nocodazole (APY266 and APY951).

(C) Legends as in (A). Cdc45-AID (mock) and Cdc45-depleted samples (APY513) are from ref. (Dumont *et al*, 2024). n = 2 biological replicates.

(D) Top: *CEN3* inactivation scheme (APY1745). Bottom: *RE* contact stripes in the *CEN3*-surrounding region. n = 1 biological replicate. Data smoothed over 10 kb.

(E) Legend as in (A). n = 1 biological replicate.

(F) Aggregated contact maps of all centromeres (top) and *RE* contact stripe in the *CEN3*-surrounding region (bottom) in WT and *chl4Δ* cells arrested in metaphase or in mitosis. Bottom: n = 1 biological replicate each. Data are from ref. (Paldi *et al*, 2020).

Figure 6: Condensin stalls at highly transcribed RNA PolII-dependent genes.

(A) From top to bottom, Hi-C contact maps, ChIP-Exo enrichment profiles of cohesin, condensin, RNA PolIII, and RNA PolII subunits (from ref. (Rossi *et al*, 2021)), detrended *RE* and rDNA-flanking contact stripes smoothed over 4 kb in asynchronous *MAT*a cells (n=5), and relevant genomic features. Contact data were obtained from cells grown in galactose-containing media while ChIP-Exo data were obtained in glucose-containing media.

(B) Hi-C matrices (top) and rDNA-flanking contact stripes smoothed over 10 kb (bottom) in the 60 kb region surrounding the *GAL2* gene in asynchronous *MAT*a cells (APY266) grown in the presence of galactose (n=5) or glucose (n=2). Bin: 1 kb.

(C) Same as (B) in *MAT*a cells (APY142) grown in YEP-lactate supplemented or not with 2% galactose or 2% glucose for 10 minutes.

(D) Same as (B) with samples used in **Fig. 5D** (containing the *pGAL-CEN3* construct).

Figure 7: DSB formation at *MAT*a blocks condensin translocation and creates a *RE*-DSB loop.

(A) Hi-C contact maps in *MAT*a and *MAT*α *rad51*Δ cells (APY1267 and APY1264, respectively) at 2 and 4 hours post-DSB induction. n = 1 biological replicate each. Bin: 1 kb.

(B) *RE* stripes in cells with an unrepairable DSB at *MAT*a or on chr. V. Data smoothed over 10 kb.

(C) Ratio of the *RE* stripes with an unrepairable DSB at *MAT*a over chr. V at 2 and 4h post-DSB induction.

(D) Ratio map of chr. III in cells with a DSB at *MAT*a over at chr. V 2h post-DSB induction.

(E) Ratio map of chr. III in cells with a DSB at *MAT*a over at *MAT*α 2h post-DSB induction.

(F) As in (B) with *MAT*α cells at 2 and 4h post-DSB induction.

(G) Ratio of *RE* stripes with an unrepairable DSB over undamaged cells in *MAT*α cells.

(H) Model for condensin-dependent chr. III folding and conditional *RE-MAT* loop establishment upon DSB formation.

(I) Roadblocks for loop extrusion by condensin in *S. cerevisiae*.

(J) Different search strategies mediated by cohesin and condensin: long-range scanning and focal search, respectively.

Methods

Haploid *S. cerevisiae* strains

Genotypes of *Saccharomyces cerevisiae* (W303 *RAD5*+ background) strains are listed in **Table S1**. The inducible *HO* expression construct *trp1::pGAL1-HO::hphMX*, the mutagenesis of the endogenous HO cut-site at *MAT* and the DSB-inducible HOcs construct *ura3::LY-HOcs* have been described previously (Piazza *et al*, 2019, 2018). The *rad51::KanMX* mutation has been obtained by transformation of a PCR fragment amplified from the relevant deletant of the Euroscarf gene deletion collection. The construct *his3::pADH1-OsTIR1-9Myc::HIS3* for OsTir1 E3-ubiquitin ligase expression, as well as the Scc1-V5-AID and Cdc45-FlagX5-AID constructs have been described previously (Piazza *et al*, 2019; Dauban *et al*, 2020). The *SMC2-AID-9Myc::NAT* and *TIR1-9Myc::URA3* constructs were described previously (Guérin *et al*, 2019). The *pGAL1-CEN2* and *pGAL1-CEN3* constructs have been described previously (Hill & Bloom, 1987; Reid *et al*, 2008).

The extended recombination enhancer (RE) on chr. III (coordinates 29,041-31,071) and its condensin peak-containing right segment (coordinates 29,865-31,071) have been introduced at inter-genic position 680,258 upon CRISPR/Cas9-mediating knock-in using guide 5'- TTGTTTCTACTAATGTGCTG -3' and repair gene fragment bearing ~150 bp of homology to each side of the break as described in (Agier *et al*, 2021). The *RE* deletion on chr. III has been obtained by CRISPR/Cas9 as described in (Dumont *et al*, 2024). Coordinates correspond to the S288c R64-2-1 *S. cerevisiae* genome assembly.

Culture media and growth conditions

- G1-arrest

Exponentially growing cultures in YEP-lactate-galactose (1% yeast extract, 1% peptone, 2% lactate, 2% galactose) were synchronized in G1 by addition of 1 µg/ml alpha-factor (GeneCust) every 30 minutes for 3 hours at 30°C prior to crosslinking.

- S-phase

Cells arrested in G1 with alpha-factor in YPD medium (1% yeast extract, 1% peptone, 2% glucose) at 30°C were washed 3 times with 50 mL of YPD and released in S-phase at 25°C for 20 minutes prior to crosslinking. For Scc1-AID depletion and Cdc45-AID depletion, 2 mM IAA was added 1 hour prior to, and in all following wash and culture media.

- Metaphase-arrest (*CDC20* repression)

Metaphase-arrest in strains in which the *CDC20* gene is placed under the control of the *pMET3* promoter (APY537) was performed as in (Dauban *et al*, 2020) with minor media differences. Exponentially growing cells in a supplemented synthetic complete lactate media deprived of methionine (0.67% yeast

nitrogen base without amino acids, 2% lactate, and supplemented with a mix of amino-acids lacking methionine) were arrested in G1 upon addition of 1 µg/ml alpha-factor (GeneCust) every 30 minutes for 4 hours at 30°C. Cells were were washed 3 times with 50 mL of YEP-lactate supplemented with 2 mM methionine, and maintained arrested in this media at 30°C for 4 hours prior to crosslinking.

- Metaphase-arrest (DNA damage checkpoint-induced)

Exponentially growing cultures in YEP-lactate medium of strains bearing the galactose-inducible *pGAL1-HO* construct for expression of the HO endonuclease and its unrepairable *HOcs* target site at *ura3* (APY266) were synchronized in G1 by addition of 1 µg/ml alpha-factor every 30 minutes for 3 hours at 30°C. Cells were washed 3 times with 50 mL of pre-warmed YEP-lactate and released in S-phase in YEP-lactate supplemented with 2% galactose to induce HO expression from the *pGAL1-HO* construct, which targets an unrepairable HOcs at *ura3* on chr. V (Piazza *et al*, 2018, 2019). In one instance, 10 µg/mL nocodazole was added to cause microtubule depolymerization. Cdc45-AID depletion was induced upon addition of 2 mM IAA 1 hour prior to release in S-phase and maintained in all media thereafter. Scc1-AID depletion was induced upon addition of 2 mM IAA upon release in S-phase and HO induction. Cells were crosslinked at 2 and 4 hours post-DSB induction.

- Mitotic-arrest (DNA damage checkpoint-induced)

Exponentially growing cultures in YEP-lactate medium at 30°C were supplemented with 10 µg/mL nocodazole and cultured an additional 4 hours prior to crosslinking.

- Induction of a DNA double-strand break at *MAT*

Exponentially growing Rad51-deficient cells (APY1264 and APY1267) in YEP-lactate medium at 30°C were supplemented with 2% galactose to induce the expression of the HO endonuclease from the *pGAL1-HO* construct. Cells were crosslinked at 2 and 4 hours post-DSB induction.

Flow cytometry

Approximately 10^7 cells were collected by centrifugation, re-suspended in 70% ethanol and fixed at 4°C for at least 24h. Cells were pelleted, resuspended in 1 mL of 50 mM sodium citrate pH 7.0 and sonicated 10 seconds on a Bioruptor. After washing, cells were treated with 200 µg of RNase A (Euromedex, cat.9707-C) at 37°C overnight. Cells were then washed and incubated for 30 minutes with 1 mL of 50 mM sodium citrate pH 7.0 with 16 µg of propidium iodide (Fisher Scientific, 11425392). Flow cytometry profiles were obtained on a MACSQuant machine and analyzed using Flowing Software 2.5.1.

Hi-C

Hi-C was conducted as described in (Dumont *et al*, 2024). Briefly, ~1.5×10^9 haploid cells were fixed with 3% formaldehyde (Sigma-Aldrich, cat. F8775) for 30 minutes at RT at 120 rpm. Formaldehyde was

quenched with 330 mM glycine for 20 minutes at RT at 120 rpm. Cells were washed twice with cold water at 3,000 g for 10 minutes. Pellets were split in two tubes and frozen at -80° C. Cell pellets were thawed in ice, resuspended in 10 mL of Zymolyase solution (0.25 mg/mL Zymolyaze 100T (Carl Roth, cat. 9329), 1 M D-sorbitol (Sigma-Aldrich, cat. S6021), 50 mM Tris-HCl pH 7.5, 10 mM 2–mercaptoethanol (Sigma-Aldrich, cat. M3148)) and spheroplasted at 210 rpm for 18 minutes at 30° C (cells spheroplasting is checked under the microscope and the incubation time adjusted accordingly). Spheroplasts are pelleted at 3,000 g for 10 minutes at 4° C, washed with 4 mL cold 1X PBS, and resuspended in a fresh EGS crosslinking solution (3 mM ethylene glycol bis(succinimidyl succinate) (Fisher Scientific, cat. 10350924) in 1X PBS), and incubated at 30° C for 40 minutes at 100 rpm. EGS was quenched with 400 mM glycine at RT for 5 minutes at 100 rpm. The crosslinked cellular material was pelleted at 3,000 g for 10 minutes at 4° C and washed twice in cold 1X PBS supplemented with anti-protease (Sigma-Aldrich, cat. 11836170001). Pellets were snap-freezed in liquid nitrogen and stored at -80°C.

The crosslinked pellets were thawed in ice and resuspended in cold H_2O supplemented with an anti-protease mix (Roche, cat. 11836170001). Between 2 and 5.10^7 cells were processed for Hi-C using the Arima Hi-C+ kit (Arima Genomics, cat. A410079) following manufacturers' instructions. The Arima Hi-C+ kit employs a dual restriction digestion (DpnII and HinfI) yielding a median fragment length of 108 bp in *S. cerevisiae.*

DNA was fragmented into 300-400 bp fragments using Covaris M220 sonicator. Preparation of the libraries for paired-end sequencing on an Illumina platform was performed using the Thermofisher Collibri ES DNA Library Prep Kit for Illumina Systems with UD indexes (cat. A38606024) following manufacturer's instructions. The library was amplified in triplicate PCR reactions using oligonucleotides corresponding to the Illumina sequence adaptors (5'-AATGATACGGCGACCACCGAGATCTACAC-3' and 5'-CAAGCAGAAGACGGCATACGAGAT-3') and Phusion DNA polymerase (New England Biolabs, cat. M0531) for 11 cycles. PCR products were purified with AMPure XP beads (Beckman-Coulter, cat. A63881) and resuspended in pure H_2O. The Hi-C library is quantified using the Qubit DNA high sensitivity kit (Thermo Scientific, cat. Q32851) on a Qubit 2 fluorometer (Thermo Scientific, cat. Q32866). Library quality control, paired-end sequencing (2x150 bp) on Illumina NovaSeq6000 or NovaSeq X Plus, and data QC were performed by Novogene UK.

Protein extraction and western blotting

Protein extracts for western blot were prepared from 5.10^7 to 10^8 cells. Cells were lysed in cold NaOH buffer (1.85 N NaOH, 7.5% v/v beta-Mercaptoethanol) for 10 minutes in ice. Proteins were precipitated upon addition of trichloroacetic acid (15% final) for 10 minutes in ice. After centrifugation at 15,000 g for

5 min, the pellets were resuspended in 100 µL of SB++ buffer (180 mM Tris-HCl pH 6.8, 6.7 M Urea, 4.2% SDS, 80 µM EDTA, 1.5% v/v Beta-mercaptoethanol, 12.5 µM Bromophenol blue). Proteins were denatured upon heating 5 minutes at 65°C. Pre-cleared extracts were resolved on 12% precast polyacrylamide gel (Bio-Rad, cat. 4561043) and blotted on a PVDF membrane (GE Healthcare, cat. 10600023). Membranes were probed with mouse anti-AID antibody (clone 1E4, CliniSciences, M214-3) diluted at 1:1000 for Cdc45-Flag-AID, an anti-GAPDH antibody (Invitrogen, MA515738) diluted at 1:10000, or an anti-V5/Pk1 monoclonal antibody (Fisher Scientific, cat. R960-25) diluted at 1:10000 for Scc1-V5-AID. Primary antibodies were revealed with an HRP-conjugated anti-mouse IgG antibody diluted at 1:10000 (Abcam, ab6789) using Immobilon Forte western HRP substrate (Merck, WBLUF0100) and a Chemidoc MP Imaging system (BioRad).

Data retrieval from SRA and GEO

Raw paired-end reads from Hi-C experiments in PRJNA526833 (Paldi *et al*, 2020), PRJNA680815 (Jeppsson *et al*, 2022), and PRJNA986466 (Jeppsson *et al*, 2024) were retrieved using the nf-core/fetchngs pipeline (nf-core/fetchngs, 2024). ChIP-Exo profiles from (Rossi *et al*, 2021) were obtained from https://www.datacommons.psu.edu/download/eberly/pughlab/yeast-epigenome-project/ (equivalent of GEO GSE147927 series).

Hi-C read alignment and generation of contact maps

Paired-end reads are aligned and processed using Hicstuff *pipeline* function in "cutsite" mode. Briefly, pairs of reads are aligned iteratively and independently using Bowtie2 in its most sensitive mode to the *S. cerevisiae* reference genome R64-2-1 with *HML*, *MAT*, *HMR*, *URA3*, *LYS2*, and the right rDNA repeat sequences were replaced by "N" of the same length (S288c_DSB_chr3_rDNA reference). In instances where a second RE fragment was introduced on chr. IV, the RE sequence on chr. III were also masked (S288c_DSB_chr3_rDNA_RE_N reference). Each uniquely mapped read was assigned to a restriction fragment. Uncuts, loops and circularization events were filtered as described in ref. (Cournac *et al*, 2012) and PCR duplicates discarded.

Generation of Hi-C ratio maps

Ratio maps were generated from sparse matrices using Hicstuff *view* function, normalized (SCN normalization) (Cournac *et al*, 2012) , log-transformed and binned. Alternatively, ratio maps were generated using Serpentine (Baudry *et al*, 2020). Briefly, two matrices binned at 1 kb of the chromosome of interest were subsampled to contain the same number of contacts. Comparison of contact maps was performed using the default threshold parameters (50 and 10) and iterated 30 times. The detrending constant was set to 0.

Generation of aggregated Hi-C contact maps

Intra-chromosomal centromere and *GAL* genes pile-ups were generated with Chromosight *quantify* with default parameters (Matthey-Doret *et al*, 2020b) from Hi-C matrices in Cooler format binned at 1 kb, subsampled at 24 million contacts and ICE-normalized.

Computation of the contact probability as a function of genomic distance

Computation of the contact probability as a function of genomic distance $P_c(s)$ and its derivative have been determined using Hicstuff *distance law* function with default parameters, averaging the contact data of entire chromosome. The mitochondrial genome and the endogenous 2μ plasmid were excluded from the analysis.

Quantification of coverage from Hi-C data

Quantification of coverage from *bam* alignment files generated with the Hicstuff *pipeline* function, which uses bowtie2 in unpaired mate mode, were sorted and merged with samtools *sort* and *merged* function. The coverage was computed over 500 bp windows without overlap using Tinycov *covplot* function. The absolute coverage per bin on chr. III was normalized onto the median coverage, and divided over that of the average of multiple samples lacking a DSB on chr. III.

Quantification of coverage from ChIP-Exo data

Quantification of coverage from *bam* alignment files following sorting with samtools *sort* function were computed as non-overlapping 20 bp bins using Tinycov *covplot* function. The resulting bedgraph files were rendered as heatmaps on IGV.

Extraction of intra-chromosomal 4C-like contact profiles

Sparse Hi-C matrices binned at 1 kb were SCN-normalized and converted to dense format using functions of the Hicstuff package. Vectors corresponding to the intra-chromosomal contacts made by the 3 kb *RE*-containing region to the right end of chr. III and the 4 kb region flanking the rDNA on the centromere-proximal side toward the left end of chr. XII were extracted and sum of contacts set to 1. For each viewpoint, 6 control viewpoints located at an equivalent distance from a centromere were selected and their contact frequency averaged. Control viewpoints for the RE, in the form chr:coordinate(strand), were V:66000(W), VIII:21000(W), XIV:713000(C), II:153000(W), XI:525631(C), XIII:182646(W). Control viewpoints for the rDNA-flanking region were IV:747000(C), XIV:332000(W), XIII:565000(C), XV:624000(C), XI:143000(W), II:536000(C).

Statistical analysis

No statistical test was performed in this study. Linear regression and data smoothing were performed under Graphpad Prism 10. Repeated elements >300 bp were excluded from the analyses. The experiments were not randomized. The investigators were not blinded to allocation during experiments and outcome

assessment. The number of times an experiment has been repeated (n) and the nature of the data representation (mean, SEM, etc.) are indicated in the figure or figure legends.

Loop extrusion model

We modeled extrusion as a unidimensional process working along the chromatin: (1) condensin can bind and unbind at a single loading site at rates k_b and k_u respectively; (2) upon binding, one leg of the condensin remains anchored at the binding site while the other translocates along the chromosome at a speed v_e. In the idealized scenario of continuous processing without boundaries or roadblocks, the distribution of loop sizes extruded by condensin, l, follows an exponential distribution (Brackley *et al*, 2017; Abdulla *et al*, 2022):

$$\rho_0(l) = \frac{1}{p} e^{-l/p} \qquad (1)$$

where $p = v_e/k_u$ is the processivity and represents the average loop size extruded by condensin when it is bound to chromatin. When an impermeable roadblock is present at site i, located a genomic distance l_i from the loading site, the loop size distribution is modified as follows:

$$\rho_i(l, l_i) = \begin{matrix} e^{-\frac{l}{p}}/p & l < l_i \\ 1 - e^{-l_i/p} & l = l_i \\ 0 & l > l_i \end{matrix}. \qquad (2)$$

Assuming a density α_i of roadblocks at block site i, the total loop size distribution for n discrete roadblocks is given by

$$\rho(l) = [\prod_{k=1}^{n}(1 - \alpha_k)]\rho_0 + \sum_{i=1}^{n}\left[\prod_{k=1}^{i-1}(1 - \alpha_k)\,\alpha_i\right]\rho_i(l, l_i). \quad (3)$$

If roadblock sites are not discrete but rather domains of width $\{\Delta l_{ki}\}$, we assume that one blocking barrier would be positioned randomly within the domain. Therefore, there are $\prod_{k=1}^{n} \Delta l_k$ different possible configurations of block site positions. To each possible configuration $\{l_i\}$ corresponds a size distribution (via Eq. (3)). The total loop size distribution is thus the mean value of $\rho(l)$ averaged over all possible block site configurations.

Given a loop size distribution, we can compute the 4C contact profile between the loading site and other genomic positions using a Gaussian polymer approximation. The contact frequency in the absence of loop extruders is described by (Halverson *et al*, 2014):

$$P_0(s) = As^{-\gamma}, \qquad (4)$$

where A is a constant, s is the genomic distance with the loading site, and γ is 1.5 for an ideal polymer and less for more compact regions (Mirny, 2011). In the presence of a fixed loop of size l, the contact probability is (Polovnikov *et al*, 2023; Polovnikov & Slavov, 2023):

$$P(s,l) = \begin{cases} A[s(l-s)/l]^{-\gamma} & s < l \\ 1 & s = l. \\ A[s-l]^{-\gamma} & s > l \end{cases} \quad (5)$$

For simplicity we assume $A = 1$. The total 4C profile is then given by:

$$P(s) = (1-d)P_0 + d\sum_l \rho(l)P(s,l) \quad (6)$$

with $d = k_b/(k_b + k_u)$ the probability to have a condensin bound at the loading site and extruding a chromatin loop.

By adjusting the parameters of the model $(p, d, \{\alpha_i\}, \{l_i\}, \{\Delta l_i\})$, we aim to achieve the best fit with experimental observations. In summary, we compare the ratio of experimental contact frequency to its corresponding control with the theoretical prediction of $P(s)/P_0(s)$. By iteratively adjusting the model parameters, we identify the optimal values. Additionally, we estimate the parameters associated with potential roadblocks by analyzing the heights, lengths, and positions of significant peaks located near these roadblocks. A jupyter python notebook describing the model and allowing to make predictions is available at https://github.com/physical-biology-of-chromatin/CondensinYeast .

Software availability

- Hicstuff (Matthey-Doret *et al*, 2020a) (version 3.1.2 available at https://github.com/baudrly/hicstuff)
- Chromosight (Matthey-Doret *et al*, 2020b) (version 1.6.3, available at https://github.com/koszullab/chromosight)
- Serpentine (Baudry *et al*, 2020) (version 0.1.3, available at https://github.com/koszullab/serpentine)
- Tinycov (version 0.3.1, available at https://github.com/cmdoret/tinycov)
- Integrative Genomics Viewer (Robinson *et al*, 2011) (version 2.8.3, available at https://igv.org)
- Bowtie2 (Langmead & Salzberg, 2012) (version 2.3.5.1 available online at http://bowtie-bio.sourceforge.net/bowtie2/)
- Samtools (Danecek *et al*, 2021) (version 1.3.1 available online at https://github.com/samtools/samtools)
- Integrative Genomics Viewer (2.8.0 available at https://igv.org)
- Cooler (Abdennur & Mirny, 2020) (version 0.9.1 available online at https://github.com/open2c/cooler)
- Flowing Software (version 2.5.1 available online at https://flowingsoftware.com/download/)

References

Abdennur N & Mirny LA (2020) Cooler: scalable storage for Hi-C data and other genomically labeled arrays. *Bioinformatics* 36: 311–316

Abdulla AZ, Vaillant C & Jost D (2022) Painters in chromatin: a unified quantitative framework to systematically characterize epigenome regulation and memory. *Nucleic Acids Res* 50: 9083–9104

Agier N, Fleiss A, Delmas S & Fischer G (2021) A versatile protocol to generate translocations in yeast genomes using CRISPR/Cas9. *Methods Mol Biol Clifton NJ* 2196: 181–198

Alipour E & Marko JF (2012) Self-organization of domain structures by DNA-loop-extruding enzymes. *Nucleic Acids Res* 40: 11202–11212

Analikwu BT, Deshayes A, Torre J van der, Guérin T, Katan AJ, Béneut C, Barth R, Phipps J, Scolari V, Veaute X, *et al* (2023) Telomere protein arrays stall DNA loop extrusion by condensin. 2023.10.29.564563 doi:10.1101/2023.10.29.564563 [PREPRINT]

Arnould C, Rocher V, Finoux A-L, Clouaire T, Li K, Zhou F, Caron P, Mangeot PE, Ricci EP, Mourad R, *et al* (2021) Loop extrusion as a mechanism for formation of DNA damage repair foci. *Nature* 590: 660–665

Arnould C, Rocher V, Saur F, Bader AS, Muzzopappa F, Collins S, Lesage E, Le Bozec B, Puget N, Clouaire T, *et al* (2023) Chromatin compartmentalization regulates the response to DNA damage. *Nature*: 1–10

Avşaroğlu B, Bronk G, Li K, Haber JE & Kondev J (2016) Chromosome-refolding model of mating-type switching in yeast. *Proc Natl Acad Sci U S A* 113: E6929–E6938

Banigan EJ, Tang W, van den Berg AA, Stocsits RR, Wutz G, Brandão HB, Busslinger GA, Peters J-M & Mirny LA (2023) Transcription shapes 3D chromatin organization by interacting with loop extrusion. *Proc Natl Acad Sci U S A* 120: e2210480120

Baudry L, Millot GA, Thierry A, Koszul R & Scolari VF (2020) Serpentine: a flexible 2D binning method for differential Hi-C analysis. *Bioinformatics* 36: 3645–3651

Bauerschmidt C, Arrichiello C, Burdak-Rothkamm S, Woodcock M, Hill MA, Stevens DL & Rothkamm K (2010) Cohesin promotes the repair of ionizing radiation-induced DNA double-strand breaks in replicated chromatin. *Nucleic Acids Res* 38: 477–487

Bell JC & Kowalczykowski SC (2016) RecA: regulation and mechanism of a molecular search engine. *Trends Biochem Sci* 41: 491–507

Belton J-M, Lajoie BR, Audibert S, Cantaloube S, Lassadi I, Goiffon I, Baù D, Marti-Renom MA, Bystricky K & Dekker J (2015) The conformation of yeast chromosome III is mating type dependent and controlled by the recombination enhancer. *Cell Rep* 13: 1855–1867

Bhalla N, Biggins S & Murray AW (2002) Mutation of *YCS4*, a budding yeast Condensin subunit, affects nitotic and nonmitotic chromosome behavior. *Mol Biol Cell* 13: 632–645

Brackley CA, Johnson J, Michieletto D, Morozov AN, Nicodemi M, Cook PR & Marenduzzo D (2017) Nonequilibrium chromosome looping via molecular slip links. *Phys Rev Lett* 119: 138101

Brandão HB, Paul P, van den Berg AA, Rudner DZ, Wang X & Mirny LA (2019) RNA polymerases as moving barriers to condensin loop extrusion. *Proc Natl Acad Sci U S A* 116: 20489–20499

Brandão HB, Ren Z, Karaboja X, Mirny LA & Wang X (2021) DNA-loop-extruding SMC complexes can traverse one another in vivo. *Nat Struct Mol Biol*

Busslinger GA, Stocsits RR, van der Lelij P, Axelsson E, Tedeschi A, Galjart N & Peters J-M (2017) Cohesin is positioned in mammalian genomes by transcription, CTCF and Wapl. *Nature* 544: 503–507

Caron P, Aymard F, Iacovoni JS, Briois S, Canitrot Y, Bugler B, Massip L, Losada A & Legube G (2012) Cohesin protects genes against γH2AX induced by DNA double-strand breaks. *PLOS Genet* 8: e1002460

Cejka P & Symington LS (2021) DNA end resection: mechanism and control. *Annu Rev Genet* 55: 285–307

Chan B & Rubinstein M (2023) Theory of chromatin organization maintained by active loop extrusion. *Proc Natl Acad Sci U S A* 120: e2222078120

Chapard C, Bastié N, Cournac A, Gadal O, Koszul R & Beckouët F (2023) Transcription promotes discrete long-range chromatin loops besides organizing cohesin-mediated DNA folding. 2023.12.29.573667 doi:10.1101/2023.12.29.573667 [PREPRINT]

Chimthanawala A, Parmar JJ, Kumar S, Iyer KS, Rao M & Badrinarayanan A (2022) SMC protein RecN drives RecA filament translocation for in vivo homology search. *Proc Natl Acad Sci U S A* 119: e2209304119

Coïc E, Richard G-F & Haber JE (2006) *Saccharomyces cerevisiae* donor preference during mating-type switching is dependent on chromosome architecture and organization. *Genetics* 173: 1197–1206

Costa A & Diffley JFX (2022) The initiation of eukaryotic DNA replication. *Annu Rev Biochem* 91: 107–131

Costantino L, Hsieh T-HS, Lamothe R, Darzacq X & Koshland D (2020) Cohesin residency determines chromatin loop patterns. *eLife* 9: e59889

Cournac A, Marie-Nelly H, Marbouty M, Koszul R & Mozziconacci J (2012) Normalization of a chromosomal contact map. *BMC Genomics* 13: 436

Covo S, Westmoreland JW, Gordenin DA & Resnick MA (2010) Cohesin is limiting for the suppression of DNA damage-induced recombination between homologous chromosomes. *PLoS Genet* 6: e1001006

Crickard JB, Moevus CJ, Kwon Y, Sung P & Greene EC (2020) Rad54 drives ATP hydrolysis-dependent DNA sequence alignment during homologous recombination. *Cell* 181: 1380-1394.e18

D'Ambrosio C, Schmidt CK, Katou Y, Kelly G, Itoh T, Shirahige K & Uhlmann F (2008) Identification of cis-acting sites for condensin loading onto budding yeast chromosomes. *Genes Dev* 22: 2215–2227

Danecek P, Bonfield JK, Liddle J, Marshall J, Ohan V, Pollard MO, Whitwham A, Keane T, McCarthy SA, Davies RM, *et al* (2021) Twelve years of SAMtools and BCFtools. *GigaScience* 10: giab008

Dauban L, Montagne R, Thierry A, Lazar-Stefanita L, Bastié N, Gadal O, Cournac A, Koszul R & Beckouët F (2020) Regulation of cohesin-mediated chromosome folding by Eco1 and other partners. *Mol Cell* 77: 1279-1293.e4

Davidson IF, Bauer B, Goetz D, Tang W, Wutz G & Peters J-M (2019) DNA loop extrusion by human cohesin. *Science* 366: 1338–1345

Dekker J, Rippe K, Dekker M & Kleckner N (2002) Capturing chromosome conformation. *Science* 295: 1306–1311

Dequeker BJH, Scherr MJ, Brandão HB, Gassler J, Powell S, Gaspar I, Flyamer IM, Lalic A, Tang W, Stocsits R, *et al* (2022) MCM complexes are barriers that restrict cohesin-mediated loop extrusion. *Nature* 606: 197–203

Dinda M, Fine RD, Saha S, Wang Z, Zang C, Li M & Smith JS (2023) Fob1-dependent condensin recruitment and loop extrusion on yeast chromosome III. *PLOS Genet* 19: e1010705

Dion V, Kalck V, Horigome C, Towbin BD & Gasser SM (2012) Increased mobility of double-strand breaks requires Mec1, Rad9 and the homologous recombination machinery. *Nat Cell Biol* 14: 502–509

Doughty TW, Arsenault HE & Benanti JA (2016) Levels of Ycg1 limit condensin function during the cell cycle. *PLOS Genet* 12: e1006216

Dumont A, Mendiboure N, Savocco J, Anani L, Moreau P, Thierry A, Modolo L, Jost D & Piazza A (2024) Mechanism of homology search expansion during recombinational DNA break repair in *Saccharomyces cerevisiae*. *Mol Cell*: S1097-2765(24)00657–9

Dyson S, Segura J, Martínez García B, Valdés A & Roca J (2021) Condensin minimizes topoisomerase II mediated entanglements of DNA in vivo. *EMBO J* 40: e105393

Freeman L, Aragon-Alcaide L & Strunnikov A (2000) The condensin complex governs chromosome condensation and mitotic transmission of rDNA. *J Cell Biol* 149: 811–824

Fudenberg G, Abdennur N, Imakaev M, Goloborodko A & Mirny LA (2017) Emerging evidence of chromosome folding by loop extrusion. *Cold Spring Harb Symp Quant Biol* 82: 45–55

Fudenberg G, Imakaev M, Lu C, Goloborodko A, Abdennur N & Mirny LA (2016) Formation of chromosomal domains by loop extrusion. *Cell Rep* 15: 2038–2049

Ganji M, Shaltiel IA, Bisht S, Kim E, Kalichava A, Haering CH & Dekker C (2018) Real-time imaging of DNA loop extrusion by condensin. *Science* 360: 102–105

Golfier S, Quail T, Kimura H & Brugués J (2020) Cohesin and condensin extrude DNA loops in a cell cycle-dependent manner. *eLife* 9: e53885

Goloborodko A, Imakaev MV, Marko JF & Mirny L (2016) Compaction and segregation of sister chromatids via active loop extrusion. *eLife* 5: e14864

Gruber S & Errington J (2009) Recruitment of condensin to replication origin regions by ParB/SpoOJ promotes chromosome segregation in *B. subtilis*. *Cell* 137: 685–696

Guérin TM, Béneut C, Barinova N, López V, Lazar-Stefanita L, Deshayes A, Thierry A, Koszul R, Dubrana K & Marcand S (2019) Condensin-mediated chromosome folding and internal telomeres drive dicentric severing by cytokinesis. *Mol Cell* 75: 131-144.e3

Guo Y, Al-Jibury E, Garcia-Millan R, Ntagiantas K, King JWD, Nash AJ, Galjart N, Lenhard B, Rueckert D, Fisher AG, *et al* (2022) Chromatin jets define the properties of cohesin-driven in vivo loop extrusion. *Mol Cell* 82: 3769-3780.e5

Haber JE (2012) Mating-type genes and *MAT* switching in *Saccharomyces cerevisiae*. *Genetics* 191: 33–64

Halverson JD, Smrek J, Kremer K & Grosberg AY (2014) From a melt of rings to chromosome territories: the role of topological constraints in genome folding. *Rep Prog Phys Phys Soc G B* 77: 022601

Heidinger-Pauli JM, Unal E, Guacci V & Koshland D (2008) The kleisin subunit of cohesin dictates damage-induced cohesion. *Mol Cell* 31: 47–56

Hill A & Bloom K (1987) Genetic manipulation of centromere function. *Mol Cell Biol* 7: 2397–2405

Hirano T (2016) Condensin-based chromosome organization from bacteria to vertebrates. *Cell* 164: 847–857

Holm C, Goto T, Wang JC & Botstein D (1985) DNA topoisomerase II is required at the time of mitosis in yeast. *Cell* 41: 553–563

Houston PL & Broach JR (2006) The dynamics of homologous pairing during mating type interconversion in budding yeast. *PLOS Genet* 2: e98

Hu J & Crickard JB (2024) All who wander are not lost: the search for homology during homologous recombination. *Biochem Soc Trans* 52: 367–377

Janissen R, Barth R, Davidson IF, Taschner M, Gruber S, Peters J-M & Dekker C (2024) All eukaryotic SMC proteins induce a twist of -0.6 at each DNA-loop-extrusion step. 2024.03.22.586328 doi:10.1101/2024.03.22.586328 [PREPRINT]

Jeppsson K, Carlborg KK, Nakato R, Berta DG, Lilienthal I, Kanno T, Lindqvist A, Brink MC, Dantuma NP, Katou Y, *et al* (2014) The chromosomal association of the Smc5/6 complex depends on cohesion and predicts the level of sister chromatid entanglement. *PLoS Genet* 10: e1004680

Jeppsson K, Pradhan B, Sutani T, Sakata T, Umeda Igarashi M, Berta DG, Kanno T, Nakato R, Shirahige K, Kim E, *et al* (2024) Loop-extruding Smc5/6 organizes transcription-induced positive DNA supercoils. *Mol Cell*: S1097-2765(24)00006–6

Jeppsson K, Sakata T, Nakato R, Milanova S, Shirahige K & Björkegren C (2022) Cohesin-dependent chromosome loop extrusion is limited by transcription and stalled replication forks. *Sci Adv* 8: eabn7063

Johzuka K & Horiuchi T (2009) The *cis* element and factors required for condensin recruitment to chromosomes. *Mol Cell* 34: 26–35

Kim E, Kerssemakers J, Shaltiel IA, Haering CH & Dekker C (2020) DNA-loop extruding condensin complexes can traverse one another. *Nature* 579: 438–442

Kim J, Wang H & Ercan S (2024) Cohesin mediated loop extrusion from active enhancers form chromatin jets in *C. elegans*. *BioRxiv Prepr Serv Biol*: 2023.09.18.558239

Kim J-S, Krasieva TB, LaMorte V, Taylor AMR & Yokomori K (2002) Specific recruitment of human cohesin to laser-induced DNA damage. *J Biol Chem* 277: 45149–45153

Kim Y, Shi Z, Zhang H, Finkelstein IJ & Yu H (2019) Human cohesin compacts DNA by loop extrusion. *Science* 366: 1345–1349

Kong M, Cutts EE, Pan D, Beuron F, Kaliyappan T, Xue C, Morris EP, Musacchio A, Vannini A & Greene EC (2020) Human condensin I and II drive extensive ATP-dependent compaction of nucleosome-bound DNA. *Mol Cell* 79: 99-114.e9

Kong X, Ball AR, Pham HX, Zeng W, Chen H-Y, Schmiesing JA, Kim J-S, Berns M & Yokomori K (2014) Distinct functions of human cohesin-SA1 and cohesin-SA2 in double-strand break repair. *Mol Cell Biol* 34: 685–698

Kostriken R & Wedeen CJ (2001) Engineered interphase chromosome loops guide intrachromosomal recombination. *EMBO J* 20: 2907–2913

Langmead B & Salzberg SL (2012) Fast gapped-read alignment with Bowtie 2. *Nat Methods* 9: 357–359

Lassadi I, Kamgoué A, Goiffon I, Tanguy-le-Gac N & Bystricky K (2015) Differential chromosome conformations as hallmarks of cellular identity revealed by mathematical polymer modeling. *PLOS Comput Biol* 11: e1004306

Lazar Stefanita L, Scolari VF, Mercy G, Muller H, Guérin TM, Thierry A, Mozziconacci J & Koszul R (2017) Cohesins and condensins orchestrate the 4D dynamics of yeast chromosomes during the cell cycle. *EMBO J* 36: 2684–2697

Lebreton J, Colin L, Chatre E & Bernard P (2024) RNAP II antagonizes mitotic chromatin folding and chromosome segregation by condensin. *Cell Rep* 43: 113901

Lengronne A, Katou Y, Mori S, Yokobayashi S, Kelly GP, Itoh T, Watanabe Y, Shirahige K & Uhlmann F (2004) Cohesin relocation from sites of chromosomal loading to places of convergent transcription. *Nature* 430: 573–578

Leonard J, Sen N, Torres R, Sutani T, Jarmuz A, Shirahige K & Aragón L (2015) Condensin relocalization from centromeres to chromosome arms promotes Top2 recruitment during anaphase. *Cell Rep* 13: 2336–2344

Li M, Fine RD, Dinda M, Bekiranov S & Smith JS (2019) A Sir2-regulated locus control region in the recombination enhancer of *Saccharomyces cerevisiae* specifies chromosome III structure. *PLoS Genet* 15: e1008339

Li Y, Lee J & Bai L (2024) DNA methylation-based high-resolution mapping of long-distance chromosomal interactions in nucleosome-depleted regions. *Nat Commun* 15: 4358

Liu S, Miné-Hattab J, Villemeur M, Guerois R, Pinholt HD, Mirny LA & Taddei A (2023) In vivo tracking of functionally tagged Rad51 unveils a robust strategy of homology search. *Nat Struct Mol Biol* 30: 1582–1591

Matthey-Doret C, Baudry L, Bignaud A, Cournac A, Montagne R, Guiglielmoni N, Foutel-Rodier T & Scolari V (2020a) koszullab/hicstuff: Use miniconda layer for docker and improved P(s) normalisation.

Matthey-Doret C, Baudry L, Breuer A, Montagne R, Guiglielmoni N, Scolari V, Jean E, Campeas A, Chanut PH, Oriol E, *et al* (2020b) Computer vision for pattern detection in chromosome contact maps. *Nat Commun* 11: 5795

Miné-Hattab J & Rothstein R (2012) Increased chromosome mobility facilitates homology search during recombination. *Nat Cell Biol* 14: 510–517

Mirny LA (2011) The fractal globule as a model of chromatin architecture in the cell. *Chromosome Res Int J Mol Supramol Evol Asp Chromosome Biol* 19: 37–51

Morao AK, Kim J, Obaji D, Sun S & Ercan S (2022) Topoisomerases I and II facilitate condensin DC translocation to organize and repress X chromosomes in *C. elegans*. *Mol Cell* 82: 4202-4217.e5

Morawska M & Ulrich HD (2013) An expanded tool kit for the auxin-inducible degron system in budding yeast. *Yeast Chichester Engl* 30: 341–351

Nakabayashi Y & Seki M (2022) Transcription destabilizes centromere function. *Biochem Biophys Res Commun* 586: 150–156

Nasmyth K (1983) Molecular analysis of a cell lineage. *Nature* 302: 670–676

nf-core/fetchngs (2024)

Orlandini E, Marenduzzo D & Michieletto D (2019) Synergy of topoisomerase and structural-maintenance-of-chromosomes proteins creates a universal pathway to simplify genome topology. *Proc Natl Acad Sci* 116: 8149–8154

Paldi F, Alver B, Robertson D, Schalbetter SA, Kerr A, Kelly DA, Baxter J, Neale MJ & Marston AL (2020) Convergent genes shape budding yeast pericentromeres. *Nature* 582: 119–123

Pelechano V, Wei W & Steinmetz LM (2013) Extensive transcriptional heterogeneity revealed by isoform profiling. *Nature* 497: 127–131

Peng XP & Zhao X (2023) The multi-functional Smc5/6 complex in genome protection and disease. *Nat Struct Mol Biol* 30: 724–734

Phipps J, Toulouze M, Ducrot C, Costa R, Brocas C & Dubrana K (2023) Cohesin complex oligomerization maintains end-tethering at DNA double-strand breaks. 2023.11.08.566226 doi:10.1101/2023.11.08.566226 [PREPRINT]

Piazza A, Bordelet H, Dumont A, Thierry A, Savocco J, Girard F & Koszul R (2021) Cohesin regulates homology search during recombinational DNA repair. *Nat Cell Biol* 23: 1176–1186

Piazza A, Koszul R & Heyer W-D (2018) A proximity ligation-based method for quantitative measurement of D-Loop extension in *S. cerevisiae*. In *Methods in Enzymology*, Spies M & Malkova A (eds) pp 27–44. Academic Press

Piazza A, Shah SS, Wright WD, Gore SK, Koszul R & Heyer W-D (2019) Dynamic processing of displacement loops during recombinational DNA repair. *Mol Cell* 73: 1255-1266.e4

Polovnikov K & Slavov B (2023) Topological and nontopological mechanisms of loop formation in chromosomes: Effects on the contact probability. *Phys Rev E* 107: 054135

Polovnikov KE, Slavov B, Belan S, Imakaev M, Brandão HB & Mirny LA (2023) Crumpled polymer with loops recapitulates key features of chromosome organization. *Phys Rev X* 13: 041029

Pradhan B, Barth R, Kim E, Davidson IF, Bauer B, van Laar T, Yang W, Ryu J-K, van der Torre J, Peters J-M, *et al* (2022) SMC complexes can traverse physical roadblocks bigger than their ring size. *Cell Rep* 41: 111491

Pradhan B, Kanno T, Umeda Igarashi M, Loke MS, Baaske MD, Wong JSK, Jeppsson K, Björkegren C & Kim E (2023) The Smc5/6 complex is a DNA loop-extruding motor. *Nature* 616: 843–848

Racko D, Benedetti F, Goundaroulis D & Stasiak A (2018) Chromatin loop extrusion and chromatin unknotting. *Polymers* 10: 1126

Reid RJD, Sunjevaric I, Voth WP, Ciccone S, Du W, Olsen AE, Stillman DJ & Rothstein R (2008) Chromosome-scale genetic mapping using a set of 16 conditionally stable *Saccharomyces cerevisiae* chromosomes. *Genetics* 180: 1799–1808

Renkawitz J, Lademann CA, Kalocsay M & Jentsch S (2013) Monitoring homology search during DNA double-strand break repair in vivo. *Mol Cell* 50: 261–272

Renshaw MJ, Ward JJ, Kanemaki M, Natsume K, Nédélec FJ & Tanaka TU (2010) Condensins promote chromosome recoiling during early anaphase to complete sister chromatid separation. *Dev Cell* 19: 232–244

Robinson JT, Thorvaldsdóttir H, Winckler W, Guttman M, Lander ES, Getz G & Mesirov JP (2011) Integrative genomics viewer. *Nat Biotechnol* 29: 24–26

Rossi MJ, Kuntala PK, Lai WKM, Yamada N, Badjatia N, Mittal C, Kuzu G, Bocklund K, Farrell NP, Blanda TR, *et al* (2021) A high-resolution protein architecture of the budding yeast genome. *Nature* 592: 309–314

Ryu J-K, Rah S-H, Janissen R, Kerssemakers JWJ, Bonato A, Michieletto D & Dekker C (2022) Condensin extrudes DNA loops in steps up to hundreds of base pairs that are generated by ATP binding events. *Nucleic Acids Res* 50: 820–832

Saad H, Gallardo F, Dalvai M, Tanguy-le-Gac N, Lane D & Bystricky K (2014) DNA dynamics during early double-strand break processing revealed by non-intrusive imaging of living cells. *PLoS Genet* 10: e1004187

Salari H, Fourel G & Jost D (2024) Transcription regulates the spatio-temporal dynamics of genes through micro-compartmentalization. *Nat Commun* 15: 5393

Sanborn AL, Rao SSP, Huang S-C, Durand NC, Huntley MH, Jewett AI, Bochkov ID, Chinnappan D, Cutkosky A, Li J, *et al* (2015) Chromatin extrusion explains key features of loop and domain formation in wild-type and engineered genomes. *Proc Natl Acad Sci U S A* 112: E6456-6465

Scherzer M, Giordano F, Ferran MS & Ström L (2022) Recruitment of Scc2/4 to double-strand breaks depends on γH2A and DNA end resection. *Life Sci Alliance* 5

Shaltiel IA, Datta S, Lecomte L, Hassler M, Kschonsak M, Bravo S, Stober C, Ormanns J, Eustermann S & Haering CH (2022) A hold-and-feed mechanism drives directional DNA loop extrusion by condensin. *Science* 376: 1087–1094

Simon P, Houston P & Broach J (2002) Directional bias during mating type switching in Saccharomyces is independent of chromosomal architecture. *EMBO J* 21: 2282–2291

Ström L, Lindroos HB, Shirahige K & Sjögren C (2004) Postreplicative recruitment of cohesin to double-strand breaks is required for DNA repair. *Mol Cell* 16: 1003–1015

Strunnikov AV, Hogan E & Koshland D (1995) *SMC2*, a *Saccharomyces cerevisiae* gene essential for chromosome segregation and condensation, defines a subgroup within the SMC family. *Genes Dev* 9: 587–599

Sullivan NL, Marquis KA & Rudner DZ (2009) Recruitment of SMC by ParB-parS organizes the origin region and promotes efficient chromosome segregation. *Cell* 137: 697–707

Tran NT, Laub MT & Le TBK (2017) SMC progressively aligns chromosomal arms in *Caulobacter crescentus* but is antagonized by convergent transcription. *Cell Rep* 20: 2057–2071

Ünal E, Heidinger-Pauli JM & Koshland D (2007) DNA double-strand breaks trigger genome-wide sister-chromatid cohesion through Eco1 (Ctf7). *Science* 317: 245–248

Valton A-L, Venev SV, Mair B, Khokhar ES, Tong AHY, Usaj M, Chan K, Pai AA, Moffat J & Dekker J (2022) A cohesin traffic pattern genetically linked to gene regulation. *Nat Struct Mol Biol*: 1–13

Vian L, Pękowska A, Rao SSP, Kieffer-Kwon K-R, Jung S, Baranello L, Huang S-C, Khattabi LE, Dose M, Pruett N, *et al* (2018) The energetics and physiological impact of cohesin extrusion. *Cell* 173: 1165-1178.e20

Wang X, Brandão HB, Le TBK, Laub MT & Rudner DZ (2017) *Bacillus subtilis* SMC complexes juxtapose chromosome arms as they travel from origin to terminus. *Science* 355: 524–527

Wike CL, Guo Y, Tan M, Nakamura R, Shaw DK, Díaz N, Whittaker-Tademy AF, Durand NC, Aiden EL, Vaquerizas JM, *et al* (2021) Chromatin architecture transitions from zebrafish sperm through early embryogenesis. *Genome Res* 31: 981–994

Wiktor J, Gynnå AH, Leroy P, Larsson J, Coceano G, Testa I & Elf J (2021) RecA finds homologous DNA by reduced dimensionality search. *Nature* 597: 426–429

Wood ER & Earnshaw WC (1990) Mitotic chromatin condensation in vitro using somatic cell extracts and nuclei with variable levels of endogenous topoisomerase II. *J Cell Biol* 111: 2839–2850

Yeh E, Haase J, Paliulis LV, Joglekar A, Bond L, Bouck D, Salmon ED & Bloom KS (2008) Pericentric chromatin is organized into an intramolecular loop in mitosis. *Curr Biol CB* 18: 81–90

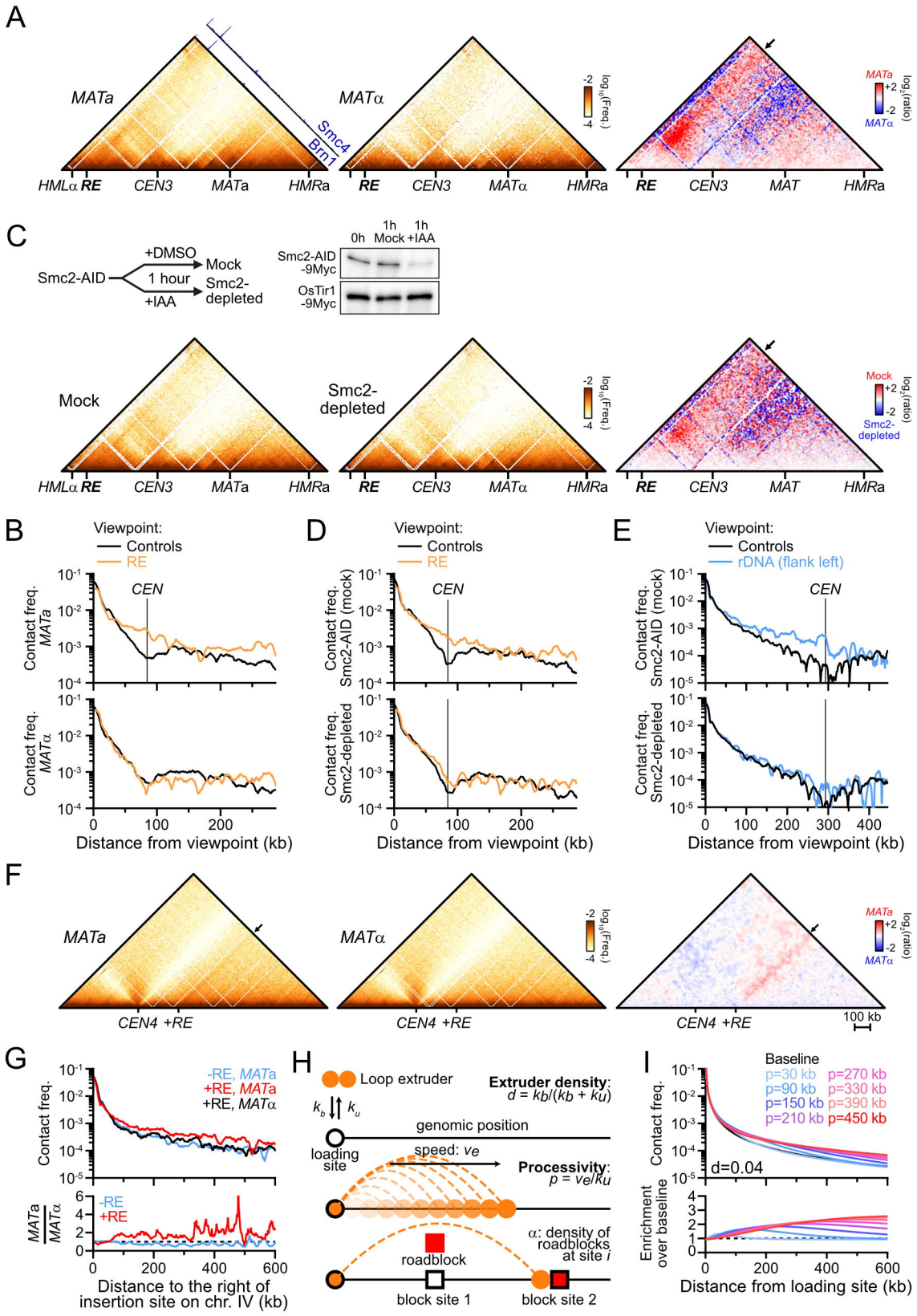
A
MATa
MATα
Smc4
Brn1
HMLα RE CEN3 MATa HMRa
RE CEN3 MATα HMRa
RE CEN3 MAT HMRa
log10(Freq.)
log2(ratio)
C
Smc2-AID
+DMSO
1 hour
+IAA
Mock
Smc2-depleted
0h
1h Mock
1h +IAA
Smc2-AID -9Myc
OsTir1 -9Myc
Mock
Smc2-depleted
B
D
E
Viewpoint:
Controls
RE
rDNA (flank left)
CEN
Contact freq. MATa
Contact freq. MATα
Contact freq. Smc2-AID (mock)
Contact freq. Smc2-depleted
Distance from viewpoint (kb)
F
CEN4 +RE
100 kb
G
-RE, MATa
+RE, MATa
+RE, MATα
Contact freq.
MATa/MATα
-RE
+RE
Distance to the right of insertion site on chr. IV (kb)
H
Loop extruder
Extruder density: d = kb/(kb + ku)
genomic position
loading site
speed: ve
Processivity: p = ve/ku
α: density of roadblocks at site i
roadblock
block site 1
block site 2
I
Baseline
p=30 kb p=270 kb
p=90 kb p=330 kb
p=150 kb p=390 kb
p=210 kb p=450 kb
d=0.04
Enrichment over baseline
Distance from loading site (kb)

Figure 1

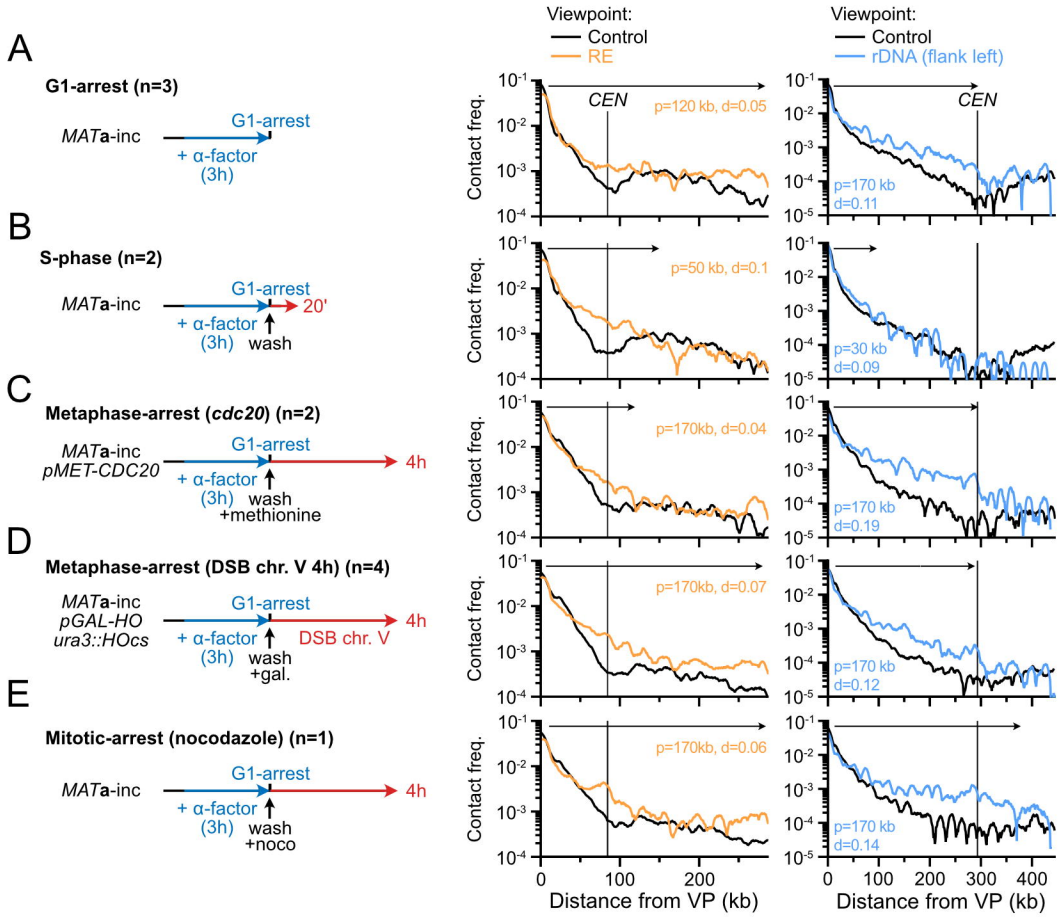
A
G1-arrest (n=3)
MATa-inc
G1-arrest
+ α-factor
(3h)
B
S-phase (n=2)
MATa-inc
G1-arrest
20'
+ α-factor
(3h)
wash
C
Metaphase-arrest (cdc20) (n=2)
MATa-inc
pMET-CDC20
G1-arrest
4h
+ α-factor
(3h)
wash
+methionine
D
Metaphase-arrest (DSB chr. V 4h) (n=4)
MATa-inc
pGAL-HO
ura3::HOcs
G1-arrest
4h
DSB chr. V
+ α-factor
(3h)
wash
+gal.
E
Mitotic-arrest (nocodazole) (n=1)
MATa-inc
G1-arrest
4h
+ α-factor
(3h)
wash
+noco
Viewpoint:
Control
RE
Viewpoint:
Control
rDNA (flank left)
CEN
p=120 kb, d=0.05
p=170 kb
d=0.11
p=50 kb, d=0.1
p=30 kb
d=0.09
p=170kb, d=0.04
p=170 kb
d=0.19
p=170kb, d=0.07
p=170 kb
d=0.12
p=170kb, d=0.06
p=170 kb
d=0.14
Contact freq.
Distance from VP (kb)

Figure 2

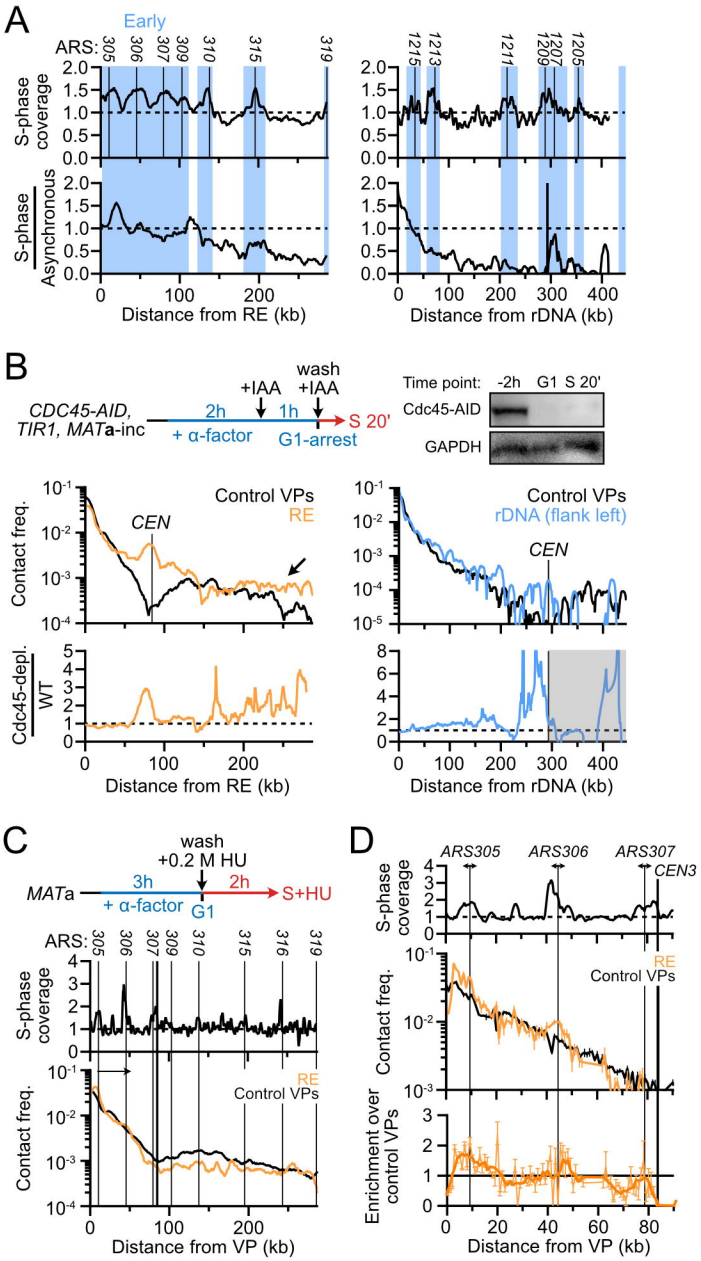
A
Early
ARS:
305
306
307
309
310
315
319
1215
1213
1211
1209
1207
1205
S-phase coverage
S-phase / Asynchronous
Distance from RE (kb)
Distance from rDNA (kb)
B
CDC45-AID, TIR1, MATa-inc
2h
+IAA
1h
wash +IAA
S 20'
+ α-factor
G1-arrest
Time point: -2h G1 S 20'
Cdc45-AID
GAPDH
Control VPs
RE
CEN
rDNA (flank left)
Contact freq.
Cdc45-depl. / WT
Distance from RE (kb)
Distance from rDNA (kb)
C
wash +0.2 M HU
MATa
3h
2h
S+HU
+ α-factor
G1
ARS:
305
306
307
309
310
315
316
319
S-phase coverage
Contact freq.
RE
Control VPs
Distance from VP (kb)
D
ARS305
ARS306
ARS307
CEN3
S-phase coverage
Contact freq.
RE
Control VPs
Enrichment over control VPs
Distance from VP (kb)

Figure 3

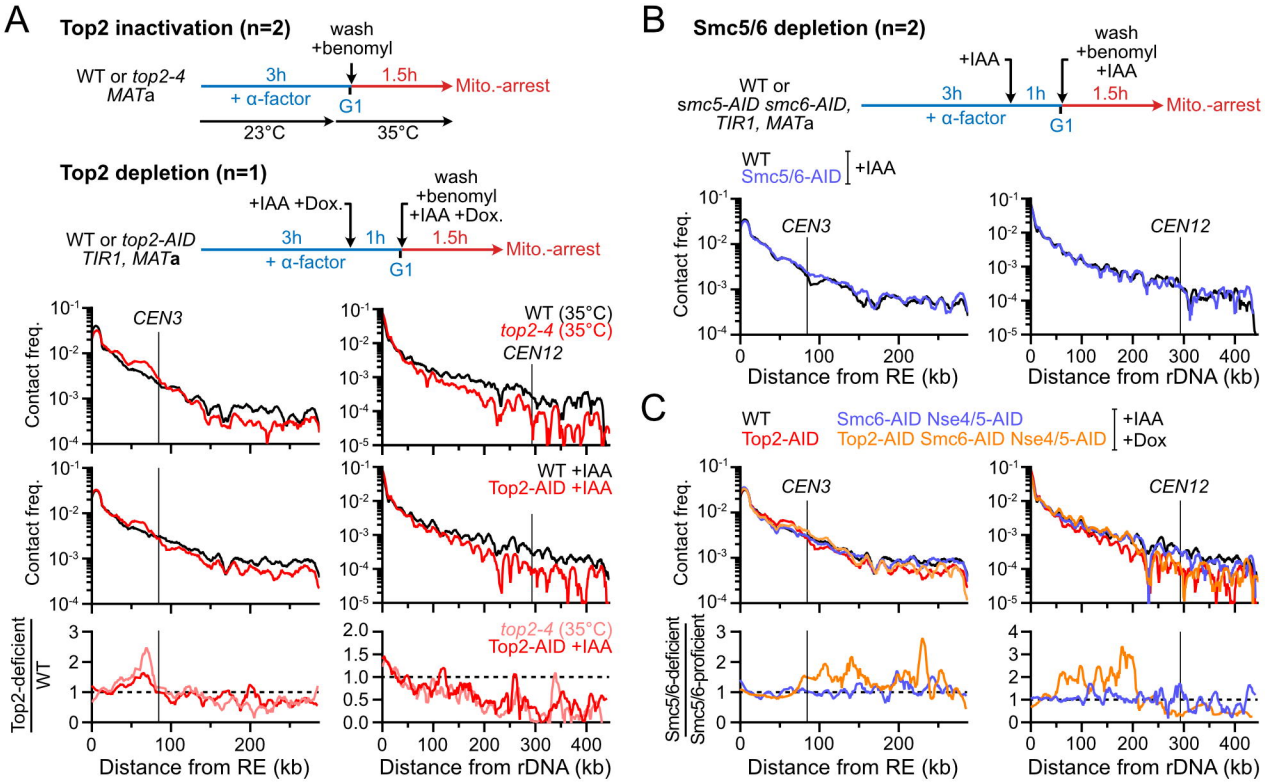
A
Top2 inactivation (n=2)
wash
+benomyl
WT or top2-4
MATa
3h
+ α-factor
1.5h
Mito.-arrest
G1
23°C
35°C
Top2 depletion (n=1)
+IAA +Dox.
wash
+benomyl
+IAA +Dox.
WT or top2-AID
TIR1, MATa
3h
1h
1.5h
Mito.-arrest
+ α-factor
G1
CEN3
CEN12
WT (35°C)
top2-4 (35°C)
WT +IAA
Top2-AID +IAA
top2-4 (35°C)
Top2-AID +IAA
Contact freq.
Top2-deficient / WT
Distance from RE (kb)
Distance from rDNA (kb)
B
Smc5/6 depletion (n=2)
+IAA
wash
+benomyl
+IAA
WT or
smc5-AID smc6-AID,
TIR1, MATa
3h
1h
1.5h
Mito.-arrest
+ α-factor
G1
WT
Smc5/6-AID
+IAA
CEN3
CEN12
Contact freq.
Distance from RE (kb)
Distance from rDNA (kb)
C
WT
Top2-AID
Smc6-AID Nse4/5-AID
Top2-AID Smc6-AID Nse4/5-AID
+IAA
+Dox
CEN3
CEN12
Contact freq.
Smc5/6-deficient / Smc5/6-proficient
Distance from RE (kb)
Distance from rDNA (kb)

Figure 4

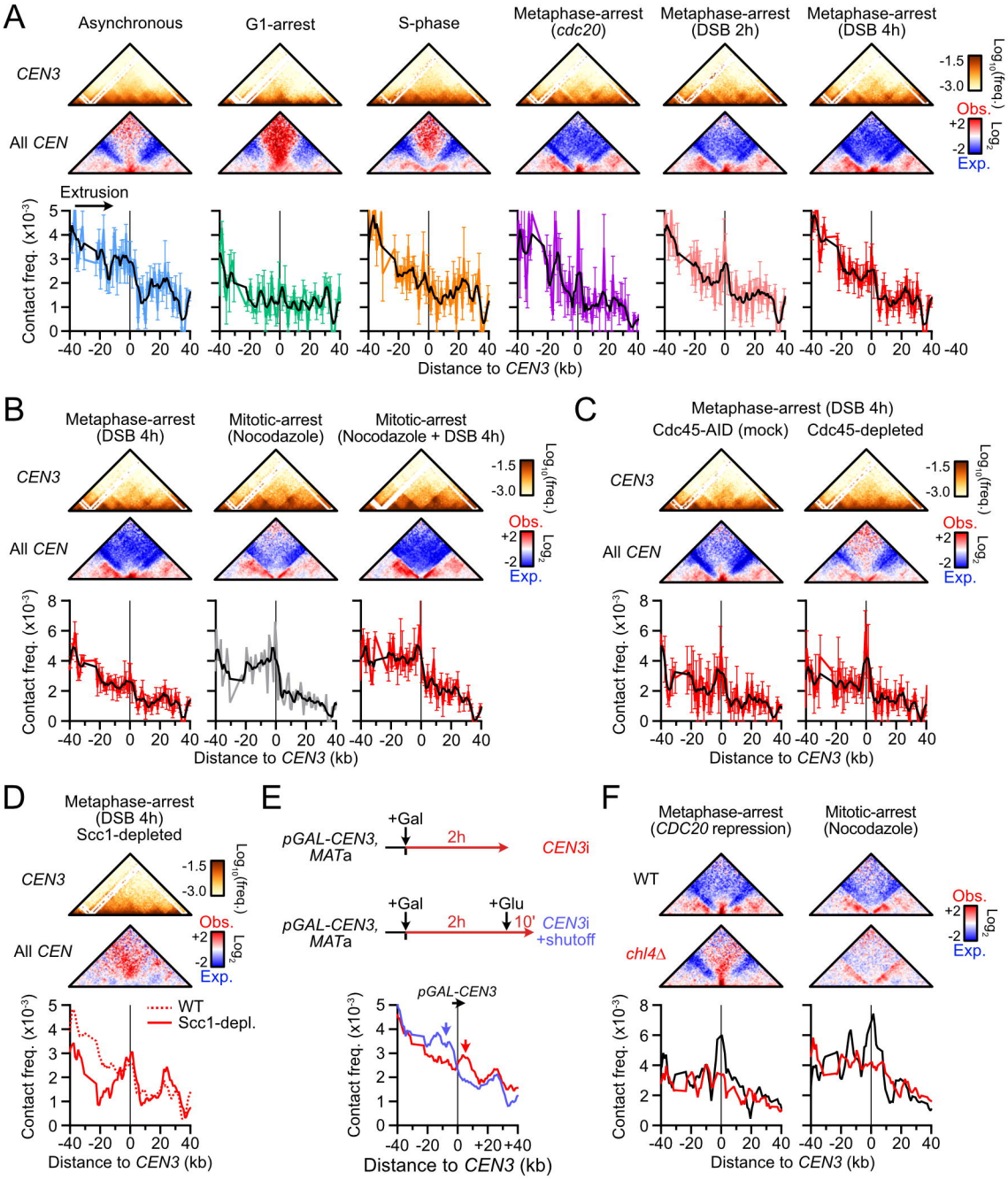
A
Asynchronous
G1-arrest
S-phase
Metaphase-arrest (cdc20)
Metaphase-arrest (DSB 2h)
Metaphase-arrest (DSB 4h)
CEN3
All CEN
Extrusion
Contact freq. (x10⁻³)
Distance to CEN3 (kb)
Log10(freq.)
Obs.
Log2
Exp.
B
Metaphase-arrest (DSB 4h)
Mitotic-arrest (Nocodazole)
Mitotic-arrest (Nocodazole + DSB 4h)
C
Metaphase-arrest (DSB 4h)
Cdc45-AID (mock)
Cdc45-depleted
D
Metaphase-arrest (DSB 4h) Scc1-depleted
WT
Scc1-depl.
E
pGAL-CEN3, MATa
+Gal
2h
CEN3i
+Glu
10'
CEN3i +shutoff
pGAL-CEN3
F
Metaphase-arrest (CDC20 repression)
Mitotic-arrest (Nocodazole)
WT
chl4Δ

Figure 5

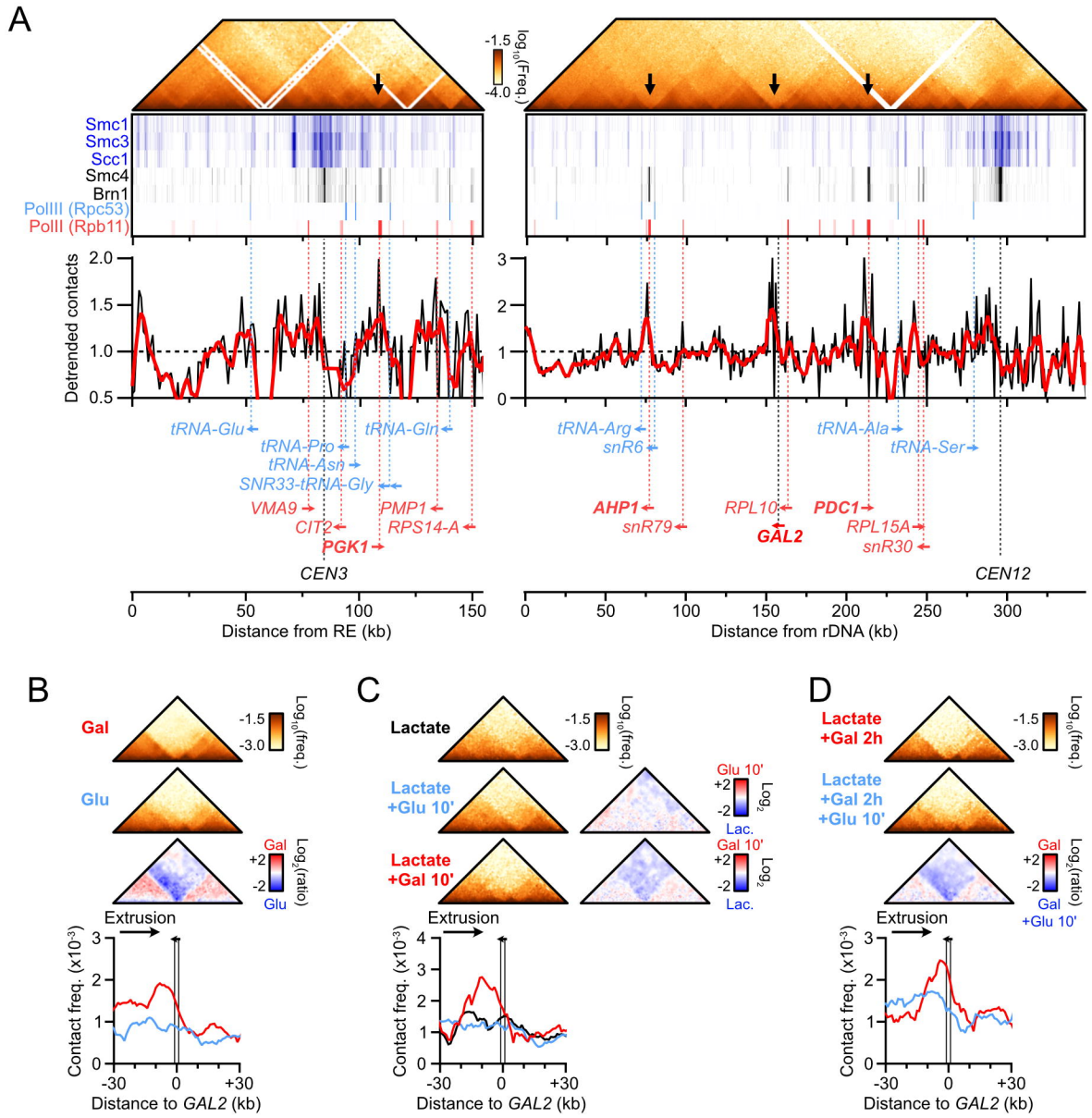
A
-1.5
-4.0
log10(Freq.)
Smc1
Smc3
Scc1
Smc4
Brn1
PolIII (Rpc53)
PolII (Rpb11)
Detrended contacts
tRNA-Glu
tRNA-Pro
tRNA-Asn
SNR33-tRNA-Gly
tRNA-Gln
VMA9
CIT2
PGK1
PMP1
RPS14-A
CEN3
Distance from RE (kb)
tRNA-Arg
snR6
AHP1
snR79
RPL10
GAL2
PDC1
RPL15A
snR30
tRNA-Ala
tRNA-Ser
CEN12
Distance from rDNA (kb)
B
Gal
Glu
Log10(freq.)
Log2(ratio)
Extrusion
Contact freq. (x10-3)
Distance to GAL2 (kb)
C
Lactate
Lactate +Glu 10'
Lactate +Gal 10'
Glu 10'
Lac.
Gal 10'
D
Lactate +Gal 2h
Lactate +Gal 2h +Glu 10'
Gal +Glu 10'

Figure 6

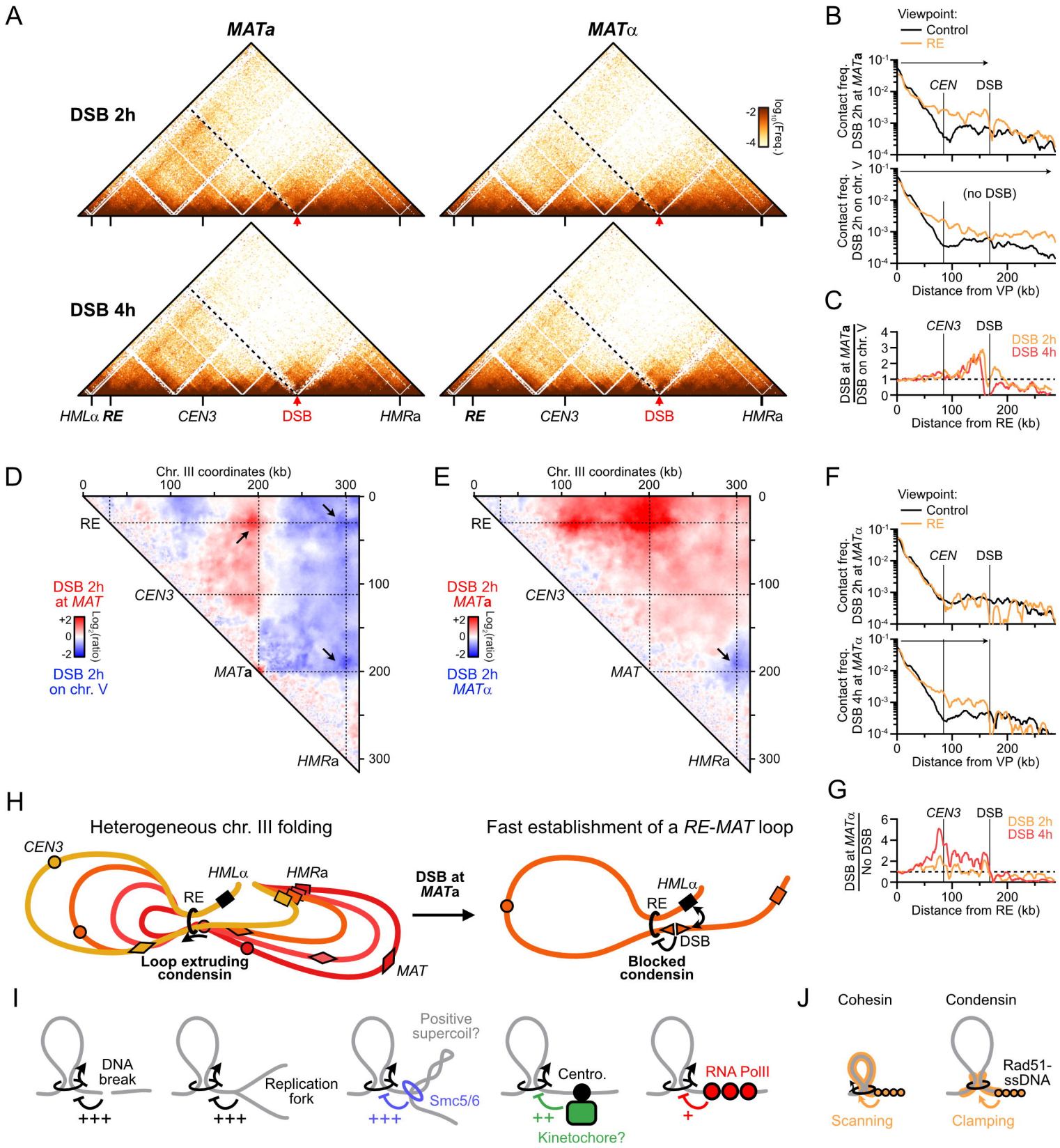
A
MATa
MATα
DSB 2h
DSB 4h
log10(Freq.)
HMLα RE
CEN3
DSB
HMRa
RE
B
Viewpoint:
Control
RE
Contact freq. DSB 2h at MATa
Contact freq. DSB 2h on chr. V
CEN
DSB
(no DSB)
Distance from VP (kb)
C
DSB at MATa / DSB on chr. V
CEN3
DSB
DSB 2h
DSB 4h
Distance from RE (kb)
D
Chr. III coordinates (kb)
RE
CEN3
MATa
HMRa
DSB 2h at MAT
DSB 2h on chr. V
Log2(ratio)
E
Chr. III coordinates (kb)
RE
CEN3
MAT
HMRa
DSB 2h MATa
DSB 2h MATα
F
Viewpoint:
Control
RE
Contact freq. DSB 2h at MATα
Contact freq. DSB 4h at MATα
CEN
DSB
Distance from VP (kb)
G
DSB at MATα / No DSB
CEN3
DSB
DSB 2h
DSB 4h
Distance from RE (kb)
H
Heterogeneous chr. III folding
CEN3
HMLα
HMRa
RE
Loop extruding condensin
MAT
DSB at MATa
Fast establishment of a RE-MAT loop
HMLα
RE
DSB
Blocked condensin
I
DNA break
+++
Replication fork
+++
Positive supercoil?
Smc5/6
+++
Centro.
++
Kinetochore?
RNA PolII
+
J
Cohesin
Condensin
Rad51-ssDNA
Scanning
Clamping

Figure 7